PLEASE CITE THIS ARTICLE AS DOI: 10.1063/5.0139179

Controlling quantum phases of electrons and excitons in moiré superlattices

Lifu Zhang^{1, #}, Ruihao Ni^{1, #}, You Zhou^{1, 2, *}

- ¹ Department of Materials Science and Engineering, University of Maryland, College Park, Maryland 20742, USA
- ² Maryland Quantum Materials Center, College Park, MD 20742, USA.
- # Equal contributions
- * Corresponding author: Y.Z.: youzhou@umd.edu

Abstract

Moiré lattices formed in twisted and lattice-mismatched van der Waals heterostructures have emerged as a platform to engineer the novel electronic and excitonic states at the nanoscale. This Perspective reviews the materials science of moiré heterostructures with a focus on the structural properties of the interface and its structural-property relationships. We first review the studies of the atomic relaxation and domain structures in moiré superlattices and how these structural studies provide critical insights into understanding the behaviors of quantum confined electrons and excitons. We discuss the general frameworks to manipulate moiré structures and how such control can be harnessed for engineering new phases of matter and simulating various quantum phenomena. Finally, we discuss routes toward large-scale moiré heterostructures and give an outlook on their applications in quantum electronics and optoelectronics. Special emphasis will be placed on the challenges and opportunities of the reliable fabrication and dynamical manipulation of moiré heterostructures.

PLEASE CITE THIS ARTICLE AS DOI: 10.1063/5.0139179

1. Overview

The electronic band theory is a widely successful theory that underpins our understanding of the electronic properties of solids and is the basis for many modern electronic technologies. However, N. F. Mott pointed out the theory's limit as it would always predict a chain of hydrogen atoms with half-filled 1s orbitals to be metallic, which is apparently wrong when the atoms are infinitely apart¹. Such a failure of the electronic band theory has been observed in a family of insulators with partially filled electronic bands, known as Mott or correlated insulators^{2, 3}. In these solids, the Coulomb interactions among electrons are stronger or comparable to the electron kinetic energy^{1, 2, 4} such that electrons cannot be treated as independent particles, which violates the basic assumption of the electronic band theory. Most interestingly, these materials can exhibit fascinating electronic properties, such as superconductivity^{5, 6}, frustrated magnetism⁷, and metal-insulator transitions⁸⁻¹¹, when they are subjected to perturbations, including doping and pressure¹²⁻¹⁴.

Understanding these emergent phenomena in correlated materials is a major challenge in condensed matter physics and requires a new theoretical framework beyond electronic band theory. However, these systems are challenging to model due to the inherent complexity of quantum many-body interactions. No analytical solutions are known for even the simplest theoretical models, such as the Hubbard model¹⁵, where one adds short-range Coulomb interactions to the tight binding model¹⁶⁻¹⁸.

The difficulty in understanding correlated systems is further exacerbated by the experimental observation that different degrees of freedom are often coupled together in these materials ¹⁹⁻²¹. Interactions among electrons and ions, such as correlation ^{1, 2, 4}, exchange ²², spin-orbit ^{23, 24}, and electron-phonon coupling ^{25, 26}, can all have similar energy scales. A small external perturbation can affect the delicate balance among these interactions and lead to phase transitions with drastic changes in the material's structural, electrical, and magnetic properties ²⁷⁻²⁹. Varying one experimental parameter, such as temperature, pressure, or doping, can often simultaneously perturb several degrees of freedom ¹⁹⁻²¹, making it difficult to understand the emergence of novel phases.

One approach to studying these complex systems is through quantum simulation³⁰⁻³³. A quantum simulator is a well-controlled many-body quantum system where one can measure the properties of the whole system, such as its conductivity, while tuning certain parameters, such as the system's Hamiltonian and doping level³²⁻³⁵. In recent years, much progress has been made toward simulating Mott-Hubbard physics using arrays of ultracold atoms confined in optical lattices³⁶⁻³⁹. In these systems, parameters such as doping level, kinetic energy, and lattice geometry can be readily controlled to investigate their effects on electronic phases^{38, 39}.

Recently, van der Waals heterostructures (vdW) made of atomically thin materials such as graphene and transition metal dichalcogenides (TMDs) have emerged as another promising platform for studying correlated electronic phenomena with highly tunable parameters⁴⁰⁻⁴⁵ (Fig. 1). These materials can be assembled into non-covalently bonded heterostructures without the constraints of lattice commensuration. Such lattice incommensuration create moiré superlattices⁴⁶ that periodically modulate atomic structure at the nanoscale. This in-plane superlattice induces local variations in the heterostructure's electronic structures, leading to the formation of minibands^{47, 48}. This effectively enhances the effective mass of the charge carriers and makes correlation effects more prominent in such vdW heterostructures. As a result, correlated electronic phases, including Mott insulators^{44, 49-53}, generalized Wigner crystals^{50, 54}, and excitonic insulators^{55, 56}, have been observed in moiré materials.

Remarkably, these moiré materials are highly tunable, with many parameters such as carrier densities, electronic band, and even band topology, controllable by experimental knobs, including external electrical field, relative interlayer twist angles, and dielectric environments. This level of control, rather unique to moiré materials, opens up exciting possibilities for the exploration of the interplay between correlation, delocalization, and topology and the potential discovery of emergent electronic phases arising from these interactions (Fig. 1).

PLEASE CITE THIS ARTICLE AS DOI: 10.1063/5.0139179

In this Perspective, we provide a perspective on how moiré materials can realize novel correlated and topological states of matter, with a particular focus on two-dimensional semiconductors. We begin by reviewing the fundamental physics of moiré superlattices in two-dimensional semiconductors. We then discuss the atomic relaxation and domain structures in moiré superlattices and how these structural studies provide critical insights into the behaviors of quantum-confined electrons and excitons. Finally, we discuss the frameworks for manipulating moiré structures and how such control can be harnessed for engineering new phases of matter and simulating various quantum phenomena that are of both fundamental interest and potential use in information and quantum technologies.

2. Introduction

2.1 vdW semiconductors and heterostructures

The ever-growing family of 2D materials⁵⁷⁻⁶⁰ offer numerous materials combinations to form moiré superlattices. Currently, the most studied vdW heterostructures hosting correlated states are made of graphene and transition metal dichalcogenides^{52, 56, 61-64}. This is partly because the high quality of their crystals and fabrication, which have been optimized over the past decade, allows for studies of pristine electronic effects in low-disorder samples⁶⁵. In this review, we will use transition metal dichalcogenides as an example system to illustrate the central ideas, and we expect that these concepts can be generalized to other vdW materials.

Transition metal dichalcogenides are a family of layered compounds with a chemical formula of MX₂, where M is a transition metal, and X can be S, Se, Te⁶⁶. Within each monolayer, a layer of transition metal atoms is bonded to and sandwiched between two layers of X atoms (Fig. 2a top panel). The TMD family with different compositions features different electronic properties. In W- and Mo- based compounds, the transition metal and chalcogenide atoms occupy the two sublattice sites of a honeycomb lattice within the 2D plane (Fig. 2a bottom panel). This broken sublattice symmetry gives rise to a bandgap at the corners of the Brillouin zone, i.e., the K and -K points⁶⁷ (Fig. 2b).

Semiconducting TMDs and their heterostructures exhibit intriguing optical properties. In TMD monolayers, the gap at K and -K points correspond to the material's direct bandgap⁶⁷⁻⁶⁹. The size of the gap ranges from 0.15 to 2.59 eV and can be tuned by alloying different transition metals and chalcogenides^{67, 70}. Optical transitions at the K and -K points have different selection rules, such that they couple to circularly polarized light of opposite chirality^{24, 71}. As a result of strong Coulomb effects and heavy masses, electrons and holes in semiconductor TMD can form tightly bound excitons, with binding energy exceeding a few hundred meVs^{67, 72}. Therefore, excitons have large oscillator strength and are the dominant optical species. Importantly excitons can interact strongly with free carriers in TMDs via various mechanisms including scattering, screening, and phase space filling⁷³. This leads to the formation of charged excitons at finite carrier doping as well as the density-dependent excitonic spectroscopic properties, such as their spectral energies and broadenings⁷⁴⁻⁷⁷. Such a correlation between electrical and optical properties of the TMDs allows for local probing of the material's conductive properties through optical studies. Furthermore, the spin-orbit coupling is strong in these materials, which leads to the spin-splitting of tens to hundreds of millielectronvolts at the K points^{24, 67}. This spin-orbit locking effect allows for the probe and manipulation of both the valley and spin degrees of freedom using light of various polarizations (Fig. 2b).

Recently, significant progress has been made in the experimental fabrication of vdW heterostructures with low disorder ⁷⁸⁻⁸⁰. The monolayer form of TMDs can be synthesized or isolated from the bulk crystals with high crystalline quality (Fig. 2c). Defect density on the order of 10¹⁰ cm⁻² has been reported ^{81, 82}. These materials can be combined in a layered fashion to form vdW heterostructures (Fig. 2d). Such heterostructures feature not only high electronic and optical qualities thanks to the lack of dangling bonds at the interface but also offer unprecedented freedom, including the twist angle engineering ^{53, 83-86}, for designing band structures.

PLEASE CITE THIS ARTICLE AS DOI: 10.1063/5.0139179

Strong correlation

One of the hallmarks of TMD thin layers is that carriers in these materials experience enhanced correlation effects compared to bulk semiconductors. On the one hand, this results from weaker screening and stronger confinement due to the reduced dimensionality ^{73, 87-89}. On the other hand, charge carriers in TMDs have relatively heavy effective mass and low kinetic energy, partly because of the *d*-orbital nature of the conduction and valence bands ^{67, 87}.

The strong Coulomb interactions and relatively weak electron kinetic energies give rise to strongly correlated behaviors even in the absence of moiré confinement potential^{55, 61, 90, 91}. This underlies recent observations of novel electronic phases in TMD heterostructures, including the formation of Wigner crystals in monolayer and coupled MoSe₂ bilayers^{61, 91}, as well as exciton insulators in coupled heterobilayers^{55, 56}. These strong correlations make these systems a promising candidate for forming exciton condensate and superfluid at high temperatures⁹².

Engineering electronic and excitonic landscape

Beyond the previously discussed correlated states featuring continuous symmetry breaking, one can impose a potential landscape on electrons or excitons to reduce their kinetic energy and engineer correlated states featuring discrete symmetry breaking. A key advantage of atomically thin materials is the easiness of creating energy landscapes. By integrating 2D materials with nanostructures, one induces a periodic pattern of strain or dielectric environment to confine electrons and enhance corelation ⁹³⁻⁹⁵. One can also subject the electrons in 2D materials to a tunable electrostatic potential by placing the 2D materials onto patterned gate dielectrics or electrodes ⁹⁶. In this Perspective, we focus on the method of imposing periodic potentials using moiré superlattice for simulating quantum systems.

2.2 Moiré superlattice – a new quantum simulating system

Moiré superlattice

A (quasi-)periodic moiré superlattice forms when the stacked two-dimensional crystals have a lattice mismatch or a misalignment of their crystallographic axes (Fig. 3a-d). The moiré lattice constants λ_m , is determined by both the lattice mismatch between the two layers δ and the relative twist angle θ (the derivation from perfect stacking, such as 0 or 60 degrees for honeycomb lattices) as:

$$\lambda_m(\theta, \delta) = \frac{(1+\delta)a}{\sqrt{2(1+\delta)(1-\cos\theta)+\delta^2}}$$

where a is the lattice constant of one of the two layers. The typical size of moiré superlattice can range from tens of nanometers to hundreds of nanometers for a few percentages of lattice mismatch or a few degrees of twist angle.

Within the moiré unit cell, the local atomic registry, i.e., stacking order, of the material varies in a periodic or quasi-periodic fashion. This variation in the local stacking order induces a spatial modulation of the material's electronic structure, such as their local band gap⁴⁸. This effect can be understood as a variation in the interlayer tunneling rates and band hybridizations for different stacking orders. Such a variation effectively imposes a potential, often called moiré potential, on both charge carriers and excitons of the materials, forming the basis of realizing quantum simulators.

Because of the broken inversion symmetry of TMD monolayers, the symmetries of the moiré superlattice can be highly dependent on the twist angle. For example, the symmetry of two stacked TMD monolayers (whether hetero- or homo-bilayers) are drastically different for $\sim 0^{\circ}$ and $\sim 60^{\circ}$ twist angles (also known as rhombohedral (R) and hexagonal (H) stacking⁶⁷) (Fig. 3a-d). The inversion symmetry is restored for $\sim 60^{\circ}$ twist (fully restored for homobilayers) while remaining broken for the $\sim 0^{\circ}$ twist, which is distinct from

PLEASE CITE THIS ARTICLE AS DOI: 10.1063/5.0139179

graphene bilayers⁴⁷. Various high symmetry points can be identified in these structures, which often feature the energy extrema of electrons and excitons (see Fig. 3 for detailed discussion). Such distinct symmetry has a profound impact on both the atomic and electronic structures of the moiré superlattice.

Lattice Reconstruction

The atomic structures of the moiré lattice can be more complicated than the above picture assuming rigid lattices without any structural relaxation. In particular, different local stacking orders can have different free energies because of the variation in the interlayer interactions ^{46, 64, 84, 97}. This can lead to both out-of-plane lattice corrugation and in-plane distortion to maximize the energetically favorable areas ^{46, 84}. However, these elastic distortions come with an energy penalty, so the atomic reconstruction is a result of the balance between interlayer interactions and intralayer lattice distortion.

As a result, the atomic reconstruction is particularly prominent at low twist angles, where only a small amount of lattice relaxation is needed^{46, 97}. This leads to the formation of domains with the lowest stacking energy separated by domain walls that are dislocations. In R and H stacking, the domains correspond to the energetically favorable stacking R_X^M and R_M^X , and R_M^X and the resulting domains have distinct shapes and symmetries (Fig.3c-d, right panels).

Various techniques have been employed to directly investigate the atomic relaxation at the nanoscale ^{46, 64, 97-100}. Electron microscopy such as transmission electron microscopy (TEM) dark-field imaging and scanning transmission electron microscopy (STEM) allow for the local determination of atomic registry and the study of domain formations (Fig. 3e-h)^{97, 99, 101}. However, they often require special sample preparation and have limitations in studying fully encapsulated devices. Recently a scanning electron microscopy (SEM) technique was developed to image domains in devices covered with thin hBN, allowing for the correlation between structural with optical and electrical properties (Fig. 3i)⁶⁴. Meanwhile, scanning probe techniques, such as conductive atomic-force microscopy (cAFM), near-field scanning optical microscopy (NSOM), and scanning tunneling microscopy (STM), which measure local electronic and optical properties, can also be used to image domain structures^{46, 98, 100, 102}. The combination of these techniques could yield critical insights into the structure-property relationship of the interface.

Experimentally it is often observed there is a variation in the domain sizes across a sample 46, 64, 97. Such a variation can arise from mechanical strain and non-uniform twist angle during the tear and stack process and can profoundly impact the electrical and optical properties of the heterostructure. Therefore, directly imaging moiré domains on fabricated devices can help to identify regions with high spatial uniformity and minimize challenges in interpreting electrical transport and optical measurements.

Quantum simulator

The variation of local atomic registry of the moiré superlattice modifies the local electronic structure of the materials, which acts as a periodic potential for electrons and excitons. The confinement potential, usually on the order of a few tens to hundreds of meVs. Such a potential is strong enough to confine quasi-particles such as electrons and excitons in the moiré unit cell, and leads to the formation of minibands. Meanwhile, the interactions among electrons and excitons can be strong due to the reduced Coulomb screening. In particular, the Coulomb interactions between electrons of neighboring moiré sites are on the order of tens to hundreds of meVs, comparable to the bandwidths of the moiré miniband^{50, 52}. Due to the strong confinement and correlation, electrons and excitons can form arrays in the moiré superlattice, a prototypical correlated state. Most remarkably, such moiré systems feature highly tunable Hamiltonian, which provides exciting avenues for simulating emergent phenomena in many-body quantum systems, including but not limited to Fermi-Hubbard and Bose-Hubbard physics (Fig. 4).

In particular, both shape and symmetry of the confinement potential can be controlled. For example, the types of lattices (such as triangular vs. honeycomb) can be chosen based on the materials combination 103 - 105 . Homobilayer will have the same potential at R_M^X and R_X^M sites, but this is not the case for a heterobilayer

This is the author's peer reviewed, accepted manuscript. However, the online version of record will be different from this version once it has been copyedited and typeset PLEASE CITE THIS ARTICLE AS DOI: 10.1063/5.0139179

due to the natural band offset^{67, 72}. This allows for the creation of a honeycomb lattice with and without sublattice symmetry. Furthermore, the same atomic lattice can host lattice potential of different geometries at different points of the Brillouin zone. For instance, compared with the often studied K points, the moiré potential at Γ points can have a six-fold rotational symmetry, which is higher than the underlying lattice¹⁰⁶.

Furthermore, the shape of the moiré potential can be readily tuned. The periodicity, λ_m , tunable over a wide range by controlling twist angle and lattice mismatch, strongly influences the interplay between localization and delocalization. In particular, there is a minimum periodicity for a given depth of confinement potential below which quasi-particles cannot be confined 103 . On the other hand, the moiré lattice constants should not be so large that the first and second minibands are no longer distinguishable $^{105,\ 107}$. Besides tuning of the moiré supercell size, the magnitude of the moiré potential, determined by the variation in the interlayer coupling, can also be controlled, such as by applying a perpendicular electric field or external pressure 51 .

Finally, the strength of the interactions between electrons and excitons can be modified. For example, reducing the unit cell size λ_m enhances the Coulomb potential but reduces the Coulomb-to-kinetic energy ratio, as the kinetic energy increases more rapidly. Furthermore, the strength of Coulomb interactions among electrons can be modulated by the dielectric environment^{93, 94, 109, 110}. Experimentally this can be achieved by placing materials of different dielectric constants near the 2D materials to introduce different screening. Recent experiments used graphene, whose carrier density can be modulated, as a tunable dielectric material to investigate the correlation effects in moiré superlattices^{111, 112}. Furthermore, the onsite interactions, when two electrons or excitons are placed within a unit cell, would increase as the moiré lattice constants decreases, providing another way to tune the correlation¹¹³. Similar techniques can also be used to manipulate the correlation among excitons, which experience van der Waals interactions and exchange interactions for intralayer excitons and dipole-dipole interactions for interlayer excitons.

3. Correlated electrons in moiré superlattice

The moiré potential can lead to correlated electronic states by reducing the electron kinetic energy via confinement and enhancing the relative strength of correlation energy. These correlated states manifest as insulating states at partial filling of the moiré minibands and were first observed in twisted bilayer graphene^{44, 114} near the magic twist angle. In contrast to graphene, the charge carriers in TMDs have a large mass, which allows for band flattening to occur over a wider range of twist angles, making the correlated states more robust, possibly occurring over a wider range of twist angles^{53, 83, 84}. Transport studies show that at half-band filling, a correlated insulator appeared that is tunable with both twist angle and displacement field (Fig. 5a)⁵³. At a 5.1° twist, zero-resistance pockets were observed on doping away from half-filling at temperatures below 3 K, indicating a possible transition to a superconducting state⁵³.

Interestingly, a perpendicular electric field applied across the vdW heterostructure can change the depth of moiré potential and dispersion of the moiré minibands, which effectively modifies the effective mass of the carriers (Fig. 5b). By controlling both the displacement field and the carrier densities, one can control the competition between electron delocalization and correlation and induce both bandwidth- and filling-controlled metal-insulator transitions^{51, 62}. This has enabled detailed investigation of the phase transition between correlated insulating states and the Fermi liquid, such as fine tuning of quantum critical transitions (Fig. 5c)^{51, 62}, which provides a system for investigating quantum critical transitions which also occur in other Mott insulators.

Beyond simple tuning of the bandwidth, the topology of the moiré minibands can also be controlled by the perpendicular electric field. When the displacement field is strong enough to reverse the band offset between two different materials, it is possible to change the orbital nature of the moiré minibands and introduce band inversion^{52, 115}. This enables the switching between a band insulator and a topological insulator and the realization of a quantum Hall insulator at full filling of the moiré minibands in a MoTe₂/WSe₂ heterostructure. Even more intriguingly, by tuning the band topology with an electric field at

PLEASE CITE THIS ARTICLE AS DOI: 10.1063/5.0139179

the half-filling, the system goes through a topological phase transition from a Mott insulator to a quantum anomalous Hall insulator ¹¹⁵ (Fig. 5d). These results demonstrate that the moiré system forms a rare platform for studying non-trivial topology in conjunction with strong correlation effects.

Optical characterizations have also proven to be a powerful tool for studying correlated states in moiré systems^{44, 49-54, 61, 116}. These methods circumvent the challenges of fabricating Ohmic contact to TMDs¹¹⁷ and can provide complimentary information on the correlated states by probing a diffraction limited spot. For instance, the exciton spectra are sensitively dependent on the concentration of free carriers, because excitons in TMDs can strongly interact with free charges and form charged excitons and Fermi polarons⁸⁸. Recent experiments have identified the discontinuity in the gate-dependent PL and reflection spectra near the half-filling of the moiré superlattice as a signature for the formation of Mott insulator¹¹⁸. Furthermore, scattering of excitons can provide critical insights into electronic and magnetic ordering of the system. For example, when electrons form a regular lattice structure in a Mott insulator, the excitons experience a periodic scattering potential which modifies the dispersion of the excitons by a umklapp process^{91, 119}. Measuring the spectral features of these umklapp peaks as a function of electron density and magnetic field could reveal both charge and magnetic ordering of the correlated states (Fig. 6a).

In addition to using excitons to probe electrons in the same layer, the excitons can also be used to remotely sense electronic states in a nearby layer (Fig. 6d)^{54, 116}. Because the binding energy of the excitons sensitively depends on the dielectric environment, a slight change in the dielectric constant or, equivalently conductivity of nearby materials can modify the excitonic energies. For example, excitons experience weaker screening from nearby insulators than metals, which results in larger binding energies. This is particularly a strong effect for the excited states because the excited states with large Bohr radius experience stronger effects of the remote layer than 1s excitons^{110, 120}. Remarkably, insulating states beyond Mott insulator and band insulator, such as generalized Wigner crystals, have been observed at factional fillings of WSe₂/WS₂ moiré lattice (Fig. 6e)⁵⁴.

Beyond transport and optical studies, other novel techniques have also been developed for studying correlated states at fractional fillings. One such technique, called optically detected resistance and capacitance (ODRC, Fig. 6b)⁵⁰, applies a high-frequency AC voltage to a gate electrode covering part of the heterostructure. Because of the high contact resistance, carriers cannot be easily injected into the heterostructure from the metal-TMD contact but rather redistribute themselves in response to the applied voltage. The redistribution current, which can be measured from the variation of the exciton spectra, provides a measurement of the sample's conductivity (Fig. 6c). Furthermore, the generalized Wigner crystal can also be visualized by scanning tunneling STM^{99, 100}, using a graphene layer as a sensor. These methods, combined with transport measurements, can provide a more complete picture of the correlated states in moiré systems.

4. Excitons in moiré superlattice

Heterostructures of vdW materials can host various types of excitons, which allows for the simulation of many-body Bosonic systems with different types of interactions (See Fig. 7). The abundance of exciton species and strong Coulomb interactions gives rise to an exciting playground for exploring novel exciton states in these materials, ranging from single photon emitter arrays and topological excitons to exciton condensates^{55, 56, 92, 103, 121}.

The effect of the moiré superlattice on excitons can be understood, to the first order, as the periodic modulation of the quasiparticle bandgap associated with the variation in the local atomic registry and corrugation. The moiré pattern can affect strongly the center-of-mass motion of excitons but influence weakly the relative motion of electrons and holes, since the moiré unit cell is larger than the exciton radius (~1–3 nm for intralayer excitons ^{110, 120}). The moiré potential is typically a few tens to hundreds of millielectronvolts ^{67, 103, 104, 122}, depending on the stacking type (H-type versus R-type), materials combination, and exciton species (intralayer versus interlayer), which traps excitons at the high symmetry

PLEASE CITE THIS ARTICLE AS DOI: 10.1063/5.0139179

points of the moiré lattice. Recent experiments suggest that a more complicated picture nay be needed when the electron and hole energy minima are located at different points in the moiré lattices. In this case, the electron and hole correlation can be significantly modified from that of free excitons, leading to a sizable spatial separation of electrons and holes and the formation of so-called charge transfer excitons 123. Nevertheless, the overall picture of spatially confined excitons remains valid. Importantly, the moirétrapped excitons can have distinct optical selection rules and optical dipoles from free excitons because of the different local stacking registries and symmetries 124. For example, valley excitons at different high symmetry points of MoX₂/WX₂ bilayers are predicted to couple to circularly polarized light with the exact opposite handedness¹⁰⁴.

Moiré trapping of excitons provides an excellent platform for simulating many-body Bosonic systems. In the low-density regime, if the interactions among the excitons are strong enough, it is possible to realize a Bose-Hubbard model, where each moiré unit cell only hosts a single or a few excitons. This creates an array of single photon emitters with potentially tunable energies and selection rules 125. Therefore, it is particularly important to engineer and enhance the strength of exciton interactions. On the other hand, in the highdensity regime, the moiré trapping can be helpful for creating exciton condensates and superfluid, which were predicted to exhibit high condensate temperatures⁹².

Another intriguing property of moiré excitons, predicted by theory, is the possible emergence of topologically non-trivial excitonic bands¹⁰⁵. In particular, electron-hole exchange interactions effectively impose an in-plane pseudo-magnetic field for the valley pseudospin and induces a valley Berry phase. The moiré potential reduces the size of the Brillouin zone and creates minibands of excitons, making it possible to have exciton bands with non-zero Chern number when the valley degeneracy is lifted by an external magnetic field¹⁰⁵.

4.1 Homobilayers

In homobilayers, interlayer hybridization modifies their electronic band structure and makes the system an indirect bandgap semiconductor^{84, 113, 126-128}. While excitons at the direct transition of K points resemble intralayer exciton, the lowest-energy excitons at the momentum-indirect gap are often a hybrid between the interlayer and intralayer excitons ^{113, 129-131}. The twist angle impacts the energetics of the direct and indirect excitons^{126, 132}, by controlling the hybridization and size of the indirect gap. Additionally, the different symmetries at around 0° versus 60° twist angles can strongly influence the excitonic behaviors. Experiments show that the K-K intralayer excitons are split into two in R-type bilayers, which are degenerate in H-type stacking 133. Similarly, the hybrid excitons at the indirect gap can have electric dipoles pointing either up or down in H-type stacking but become layer polarized in R-type stacking (Fig. 8a-b)¹³³. These effects can be understood as an out-of-plane polarization associated with the broken mirror and inversion symmetry in Rtype stacking. Remarkably recent experiments show that an external electric field can flip this out-of-plane polarization by inducing an in-plane sliding motion between the two layers (Fig. 8c)¹³⁴. This effectively functions as a ferroelectric material and provides a powerful way to tune the electronic and excitonic properties^{134, 135}.

These observations provide critical insights for understanding excitons in homobilayer moiré superlattice. When the lattice reconstruction effect is strong, twisted homobilayers can be thought of as a series of perfectly stacked domains separated by domain walls. The motion of excitons in these domains can be impeded by the domain walls. Recent experiments used a SEM technique to image the domains in the twisted WSe₂ homobilayers⁶⁴ and correlate their optical properties with domain sizes. It was found that direct excitons at the higher energy can move to the lower-energy position leading to single peak emission (Fig. 8d). This occurs if the moiré periodicity is small (< 10 nm) so that the excitons can reach the lower energy position before they recombine.

4.2 Heterobilayers

This is the author's peer reviewed, accepted manuscript. However, the online version of record will be different from this version once it has been copyedited and typeset. PLEASE CITE THIS ARTICLE AS DOI: 10.1063/5.0139179

In most heterobilayers, a type-II staggered band alignment forms at the interface featuring strong charge transfer based on first-principal calculations^{67, 136-138}. The lowest energy excitons are spatially indirect with lower oscillator strength and longer lifetime compared with intralayer excitons¹³⁹⁻¹⁴³. These interlayer excitons can be both momentum direct or indirect, dependent on the materials combination and the twist angle^{137, 138}.

Experimentally it has been observed that interlayer excitons in moiré superlattice exhibit multiple peaks with equal energy spacing, which was attributed to the quantized exciton levels due to the confinement effects (Fig. 9a)¹⁴⁴. Interestingly, very sharp excitonic PL emission has been observed at low excitation power, with linewidths of ~100 μ eV in a MoSe₂/WSe₂ heterobilayer (Fig. 9b)¹⁴⁵. Recent experiments show that the photons emitted exhibit antibunching behaviors, with a sub-unity second order correlation function $g^{(2)}(0) = 0.28 \pm 0.03$ (Fig. 9c), which suggests single photon emission from these sharp peaks¹⁴⁶.

On the other hand, reflection measurements often probe the momentum-direct intralayer excitons due to their larger oscillator strength, often at higher energy than interlayer excitons. In WSe₂/WS₂ and MoSe₂/WS₂ heterobilayers, the intralayer excitons of the selenides are split into three peaks separated by ~100 meV and ~70 meV (Fig. 9d), respectively^{63, 147}, indicating strong moiré potential. A rich variety of intralayer moiré excitons can exist. For example, under a vertical electric field, certain moiré excitons exhibit energy shift and anti-crossing behaviors, suggesting that they are layer-hybridized rather than purely intralayer¹⁴⁸. Furthermore, density-dependent reflection spectra show that moiré excitons can be either Wannier with electron and hole wavefunctions located at the same high symmetry points or charge-transfer excitons with the hole and electron located at different positions of the moiré unit cell¹⁴⁷.

One common challenge in fully understanding moiré excitons, however, is related to inhomogeneous twist angle and domain sizes, discussed in Section 2. The non-uniform strain distribution can split the exciton peak into multiple ones, making it difficult to attribute the observed phenomena to an ideal moiré superlattice. To address this issue, it is important to fabricate and identify samples with homogeneous domain sizes using various imaging techniques. The moiré effects can also be verified by varying the moiré periodicity, which should change the energy splitting of moiré excitons. Additionally, polarization-resolved PL measurements can provide important insights into the origins of the PL peaks as random strains can modify the selection rules¹⁴⁵.

5. Challenges and outlook

A central materials challenge in the study of moiré physics is the non-uniform twist angle across the heterostructure. Such variations in the twist angle can be a major source of disorder that needs to be carefully considered to fully understand moiré physics. On the one hand, one can combine techniques such as SEM and SNOM to establish the local intrinsic structure-property relationships of moiré superlattices. Another intriguing approach is to dynamically control the twist angle by rotating one layer on top of another, as has been demonstrated in several vdW heterostructures of graphene and hBN (Fig. 10a-c). Dynamically varying the global twist angle offers a promising route for systematically investigating the structural-properties relationship in a single device^{149, 150}, if this technique can produce highly homogeneous samples in various materials. Furthermore, in-plane bending of a single component layer can intentionally create twist angle variation, likely in a more controlled fashion¹⁵¹. These methods for continuous tuning of twist angels with high spatial homogeneity can will be essential for investigating the structural-properties relationship in a single device^{149, 150},

Beyond understanding the roles of twist angle variations, various approaches need to be explored to minimize angular disorders during stacking. For example, automated transfer techniques with precise motion and temperature control might reduce twist variation by rendering less strain buildup during the stacking while increasing the throughput. Mechanical cleaning at an elevated temperature ^{152, 153} can help remove blisters from fully formed heterostructures and reduce interfacial disorders. Robotic stack assembly in vacuum also helps to create pristine interfaces and could be promising for fabricating heterostructures

PLEASE CITE THIS ARTICLE AS DOI: 10.1063/5.0139179

with a high level of spatial uniformity ¹⁰¹. Suspended heterostructures allow for the isolation of the materials from substrate disorders and clamping, and can be integrated into electromechanical devices for dynamical strain control ¹⁵⁴⁻¹⁵⁹. The proper choice of material combinations can also contribute to ameliorating this issue. The higher stiffness of multilayer 2D materials compared with monolayers could lead to less strain buildup and more homogeneous domains ^{160, 161}. In heterostructures with large lattice mismatch, the moiré superlattice constant and their electronic structures are less sensitive to the twist angle, providing another way to circumvent this challenge ^{51, 52, 115}.

Direct synthesis of vdW heterostructure, such as by chemical vapor deposition, may avoid some issues associated with the stochastic nature of the mechanical stacking process. However, the exact synthesis of arbitrary twist angle remains difficult despite significant recent progress (Fig. 10d-i)^{126, 162-164}. One way to achieve better control over twist angles is to leverage growth kinetics, dislocations, lattice mismatch, and external strain¹⁶⁴⁻¹⁶⁶. Meanwhile growing perfectly aligned heterostructure which is thermodynamically stable, is another promising route for realizing moiré superlattices with minimal angular disorder. As a result, efforts to improve the direct synthesis of monolayers, which typically contain more disorders than exfoliated ones at present, will be critical.

From a fundamental scientific perspective, moiré materials with such remarkable tunability, will continue to enable the access of various many-body phenomena in both fermionic and bosonic systems. The correlated states can feature tunable spin Hamiltonians in different lattice geometries and can be used to simulate frustrated magnetic states and fractionalized spin liquids ^{106, 167}. A variety of collective phases can be realized in a single device, including exciton insulators ^{55, 56}, exciton condensates ⁹², and even Wigner supersolids ¹²¹, allowing us to investigate how these phases compete in the quantum regime. Electrical and magnetic manipulation of electrons and excitons allows for detailed investigation of the interplay between correlation, delocalization, and topology. An intriguing question is whether one can coherently control the properties of individual electrons and excitons, such as their spins and valleys, like in an atomic array. If successful, this not only create an exciting system for entangling a large number of particles that could be useful for both quantum science and technology ¹⁶⁸.

The quantum states of electrons and excitons in moiré materials offer enormous potential for novel technological applications. For example, the realization of superfluid and superconductivity in moiré materials could enable voltage control of dissipationless current flow, which may form the foundation for novel electronic and optical switches. Similarly electrical control of excitonic flow enables excitonic devices for optoelectronics ^{169, 170}. The topological exciton band in moiré materials can lead to valley-polarized edge exciton flow without backscattering ¹⁰⁵, which can have applications in classical and quantum optoelectronics. When embedded in cavities, the interactions among moiré excitons can be further enhanced for nonlinear and quantum optical applications ^{171, 172}. The quantum emitter arrays provide an electrically tunable source for single photons, and an external electric field can control the positioning of the emitters in the moiré pattern while inverting their optical selection rules ¹⁰³. This enables the generation of circularly polarized single photons and the potential creation of a spin-photon interface.

Beyond TMD- and graphene-based heterostructure, we expect that the exploration of new material systems and innovative device architectures will further expand the potential for discovery in stacked heterostructures. Collaborative efforts between chemists, physicists, and materials scientists will be crucial in advancing the field of moiré materials and realizing these potential applications. With these efforts, the study of quantum phenomena in moiré materials has the potential to unlock new possibilities for engineering and controlling quantum systems.

ACKNOWLEDGMENTS

PLEASE CITE THIS ARTICLE AS DOI: 10.1063/5.0139179

L.Z. and Y.Z. are supported by the U.S. Department of Energy, Office of Science, Office of Basic Energy Sciences Early Career Research Program under Award Number DE-SC-0022885. R.N. and Y.Z. acknowledge support from the National Science Foundation (NSF) CAREER Award under Award Number DMR-2145712.

AUTHOR DECLARATIONS

Conflict of Interest

The authors have no conflicts to disclose.

DATA AVAILABILITY

The data that support the findings of this study are available from the corresponding author upon reasonable request.

This is the author's peer reviewed, accepted manuscript. However, the online version of record will be different from this version once it has been copyedited and typeset.

PLEASE CITE THIS ARTICLE AS DOI: 10.1063/5.0139179

Fig. 1 Emergent phases arising from the interplay between correlation, fluctuations, and topology in moiré superlattice.

topological exciton superconductivity generalized Wigner crystal frustrated magnetism Mott insulator

This is the author's peer reviewed, accepted manuscript. However, the online version of record will be different from this version once it has been copyedited and typeset. PLEASE CITE THIS ARTICLE AS DOI: 10.1063/5.0139179

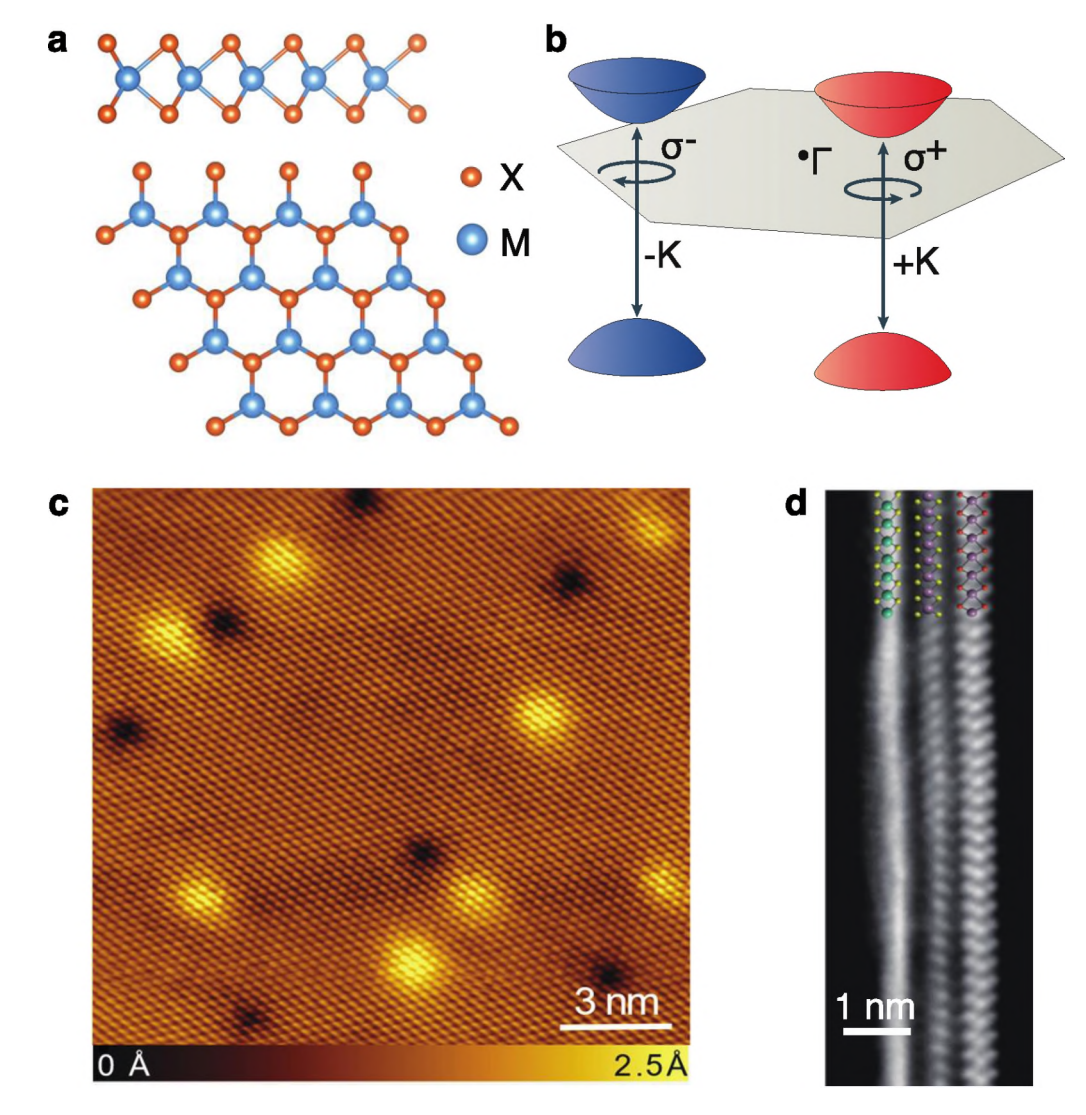


Fig. 2 Crystal structure and band structure of transition metal dichalcogenides (TMDs) and their heterostructures. a, Atomic structures of monolayer TMDs. b, Direct bandgap and optical selection rule in typical monolayer TMD. c, High-resolution STM topographic images of MoSe₂. d, Cross-sectional STEM image of a MoSe₂/MoS₂/WS₂ heterostructure with the electron beam aligned with the armchair axis of MoSe₂ (right) and MoS₂ (middle). Panels adapted with permission from: c, Reproduced with permission from Edelberg *et al.*, Nano Lett. 19, 4371 (2019). Copyright 2019 American Chemical Society; d, Reproduced with permission from Kang *et al.*, Nature 550, 229-233 (2017). Copyright 2017 Springer Nature Ltd.

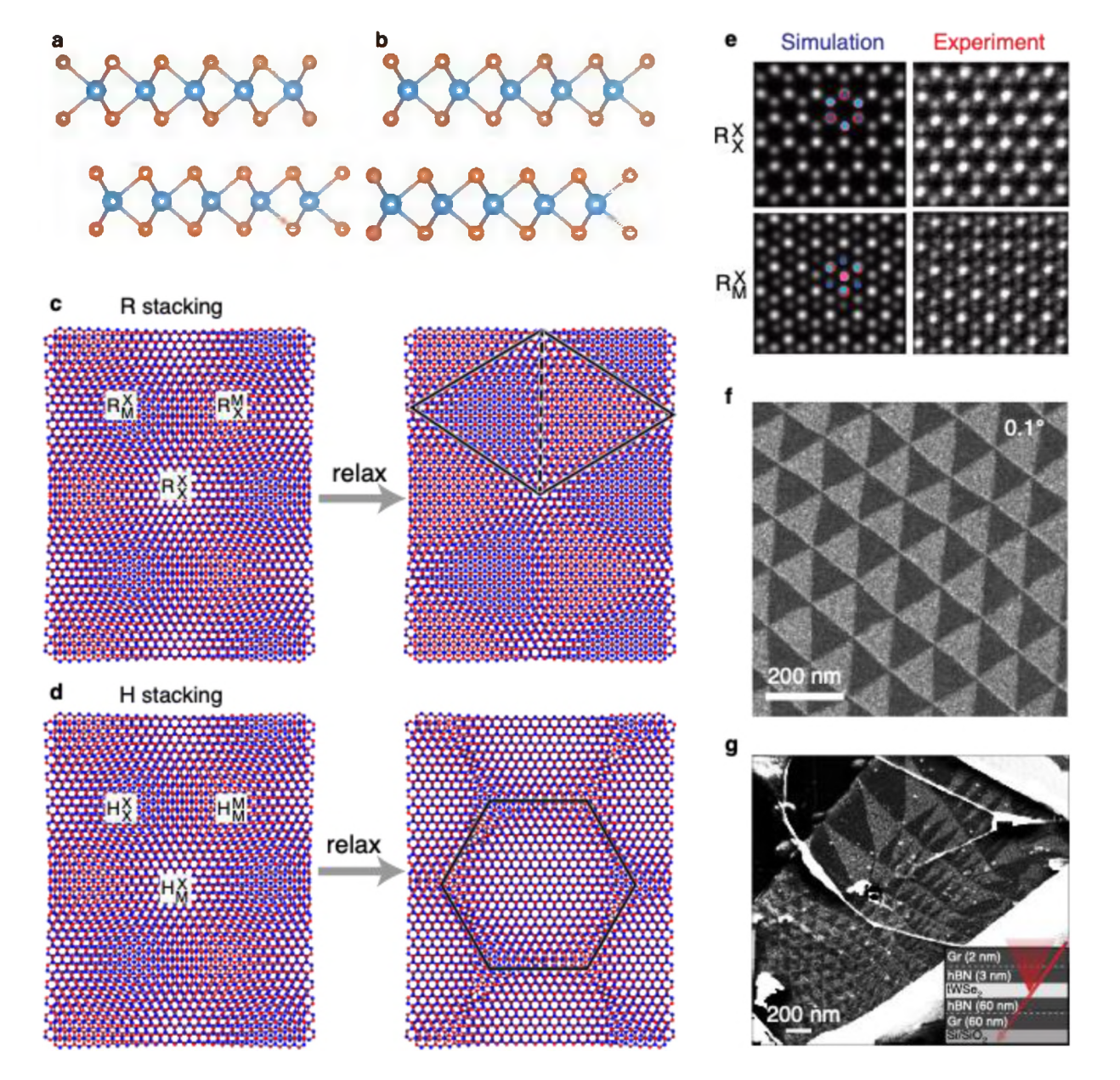


Fig. 3 Stacking order and lattice reconstruction of moiré superlattices. a, b, Sideview of 2H vs. 3R stacking. c, Moiré lattice for R stacking before and after relaxation. d, Moiré lattice for H stacking before and after relaxation. The symmetry group of the moiré superlattice would be a subset of the individual component lattice. The overall symmetry of the superlattice can be identified by examining the high symmetry points of the moiré lattice which also often correspond to the critical points of stacking-dependent electronic properties. The 0° or rhombohedral stacking feature three high symmetry points, R_X^X , R_M^X , and R_X^M . R_X^X is the perfectly aligned point with overlapping chalcogenide (X) atoms (R_M^M is close and practically identical to R_X^X). At R_M^X (R_X^M), an X atom from one layer is directly over (below) an M of the other layer in a so-called Bernal stacking 46. The local mirror symmetry, with a mirror plane between the two layers, is broken at both R_M^X and R_X^M , but restored at R_X^X . Similarly, the high symmetry points of the H stacked bilayer can be identified and named as H_X^X , H_M^M , and H_M^X . In both cases, the moiré superlattice can be viewed as a triangular lattice of perfectly stacked region (R_X^X and H_M^X) surrounded by a honeycomb lattice made of two types of stacking (R_X^M and R_M^X , H_X^X and H_M^M , respectively). **e**, Moiré pattern on an R-stacked MoS₂/WSe₂

ACCEPTED MANUSCRIPT

Journal of Applied Physic



This is the author's peer reviewed, accepted manuscript. However, the online version of record will be different from this version once it has been copyedited and typeset.

PLEASE CITE THIS ARTICLE AS DOI: 10.1063/5.0139179

heterobilayer as revealed by STEM. **f**, TEM dark-field image of twisted bilayer graphene with a twist angle of 0.1°. **g**, SEM image of a twisted bilayer WSe₂ showing a reconstructed moiré pattern with triangular AB and BA (3R) stacking domains. Panels adapted with permission from: **e**, Reproduced with permission from Zhang *et al.*, Sci. Adv. **3**, e1601459 (2017). Licensed under a Creative Commons Attribution (CC BY) license; **f**, Reproduced with permission from Yoo *et al.*, Nat. Mater. **18**, 448-453 (2019). Copyright 2019 Springer Nature Ltd; **g**, Reproduced with permission from Andersen *et al.*, Nat. Mater. **20**, 480-487 (2021). Copyright 2021 Springer Nature Ltd.

This is the author's peer reviewed, accepted manuscript. However, the online version of record will be different from this version once it has been copyedited and typeset. PLEASE CITE THIS ARTICLE AS DOI: 10.1063/5.0139179

 λ_{m} density E-field, pressure λ_m' twist, mismatch dielectric environment

Fig. 4 Tunable parameters in a moiré quantum simulator. λ_m : lattice constant of a moiré superlattice. E_m : depth of moiré potential. U: on-site Coulomb interaction. t: kinetic energy. J: exchange interaction. ε : dielectric constant. Changing one physical parameter sometimes influences several parameters in the Hamiltonian. For instance, decreasing the moiré lattice size λ_m increases both the kinetic energy t and the Coulomb repulsion U.

PLEASE CITE THIS ARTICLE AS DOI: 10.1063/5.0139179

This is the author's peer reviewed, accepted manuscript. However, the online version of record will be different from this version once it has been copyedited and typeset

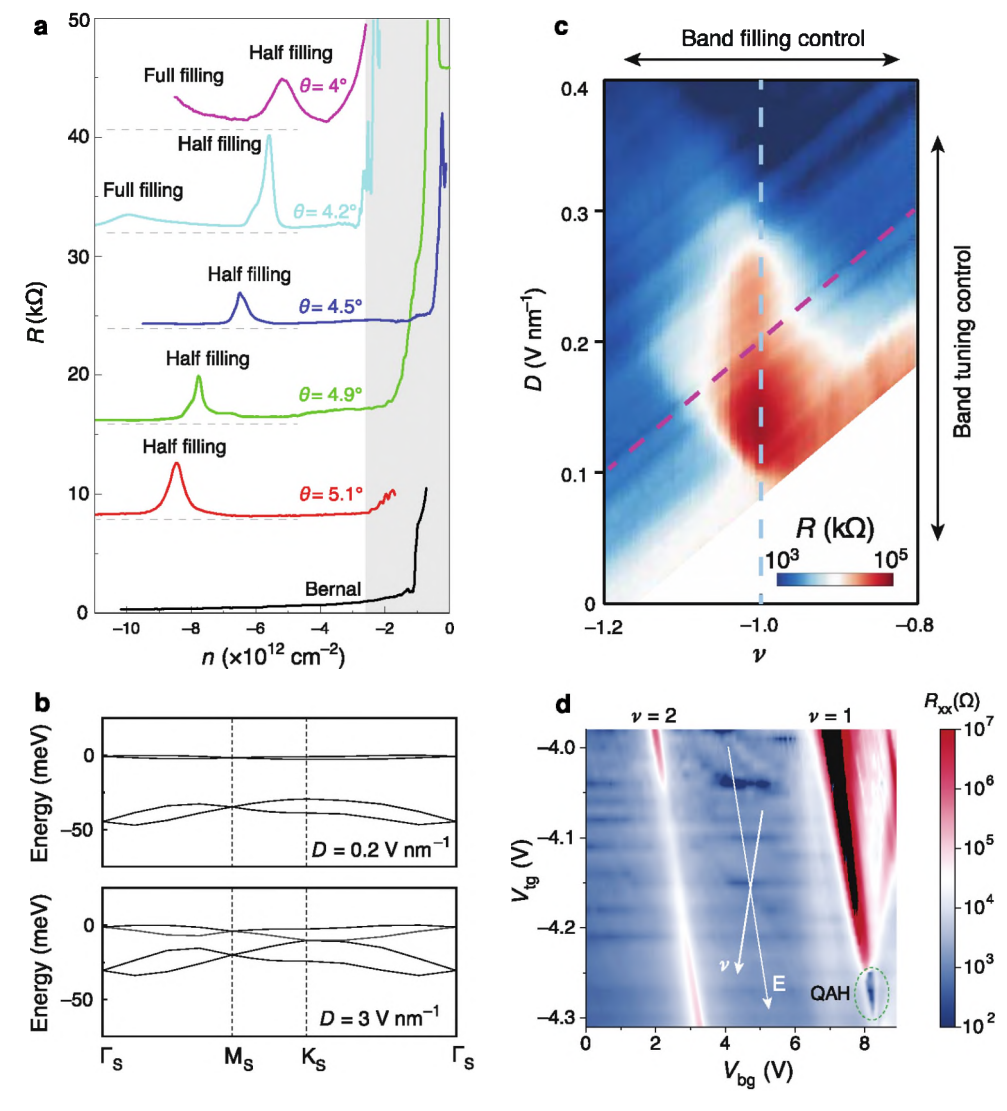


Fig. 5 Correlated electronic phases in moiré superlattice. a, Resistance as a function of carrier density n for WSe₂ homobilayers with different twist angles revealing correlated states. All are measured at 1.8 K. The dashed lines refer to the zero resistance for each curve. b, DFT calculations showing a displacement field modifies the dispersion of the hole moiré bands of a MoTe₂/WSe₂ heterobilayer. c, Bandwidth- and filling controlled metal-insulator transition. Resistance as a function of displacement field D and band filling ν for a WSe₂ homobilayer with a twist angle of 4.2°. The band filling ν is defined in units of electrons per unit cell of the moiré superlattice. All data are collected at 1.6 K. d. Ouantum anomalous Hall states emerging in an AB-stacked MoTe₂/WSe₂ heterobilayer. Longitudinal resistance of as a function of top and bottom gate voltages drops to near zero near quantum anomalous Hall insulator in the dashed circle region. V_{tg} and V_{bg} control the filling factor ν and displacement field E independently along the white arrow directions. All data are collected at 0.3 K. Panels adapted with permission from: a, Reproduced with permission from Wang et al., Nat. Mater. 19, 861-866 (2020). Copyright 2020 Springer Nature Ltd. b. Reproduced with permission from Li et al., Nature 597, 350-354 (2021). Copyright 2021 Springer Nature Ltd, c, Reproduced with permission from Ghiotto et al., Nature 597, 345-349 (2021). Copyright 2021 Springer Nature Ltd; **d**, Reproduced with permission from Li et al., Nature **600**, 641-646 (2021). Copyright 2021 Springer Nature Ltd.

ng Applied Physics

This is the author's peer reviewed, accepted manuscript. However, the online version of record will be different from this version once it has been copyedited and typeset

PLEASE CITE THIS ARTICLE AS DOI: 10.1063/5.0139179

 n/n_0 þ Region 1 Region 2 1.2 3.0 Δñ 2.5 1.0 ∆OC (×10-4) S ~ 2.0 0.6 0.4 0.5 -1.0 -1.5 V_{top} (V) 1.640 0 -2.0 -2.5 -3.0 1.630 1.635 Energy (eV) d $\frac{4}{3} \frac{3}{2} \frac{5}{3}$ 1.87 top gate (%) 1.86 1.85 1.84 hBN hBN spacer hBN 1.82 v_g (v) 10 back gate

Fig. 6 Optical characterizations for correlated states in moiré systems. a, Chemical potential dependence of the differential reflectance (with respect to energy E) of a MoSe₂/hBN/MoSe₂ homobilayermoiré heterostructure. Umklapp exciton resonances can be observed near the half-filling. b, Schematic for ODRC measurement in a WSe₂/WS₂ heterostructure. A high-frequency AC voltage applied to region 1 leads to charge redistribution between region 1 and 2. The corresponding variation in the carrier densities in region 2 can be optically detected via a lock-in measurements. C₁, C_B and C₂ are the geometric capacitances of the system while R and C₀ are the doping-dependent resistance and quantum capacitance of region 1, respectively. c, Resistance and capacitance values extracted from ODRC signal of a WSe₂/WS₂ heterostructure at different frequencies as a function of doping density. d. Schematic of the device structure utilizing Rydberg excitons for the detection of correlated states. e, A series of insulating states in a WSe₂/WS₂ heterobilayer are revealed by blueshifts of the 2s exciton resonance of a remoted WSe₂, accompanied by an enhancement in the spectral weight. Panels adapted with permission from: a, Reproduced with permission from Shimazaki et al., Phys. Rev. X. 11, 021027 (2021). Licensed under a Creative Commons Attribution (CC BY) license; b, c, Reproduced with permission from Regan et al., Nature 579, 359-363 (2020). Copyright 2020 Springer Nature Ltd: d, e, Reproduced with permission from Xu et al., Nature **587**, 214-218 (2020). Copyright 2020 Springer Nature Ltd.

This is the author's peer reviewed, accepted manuscript. However, the online version of record will be different from this version once it has been copyedited and typeset PLEASE CITE THIS ARTICLE AS DOI: 10.1063/5.0139179

Fig. 7 (a) Schematics of intralayer and interlayer excitons. The intralayer excitons behave similarly to their monolayer counterparts but experience additional effects from the neighboring materials. The interlayer excitons featuring spatial separation of the electron and hole have weaker oscillator strength and permeant dipoles^{173, 174}. Therefore, they have longer radiative lifetime and their energies can be tuned by electric-field via a Stark effect^{86, 130, 139, 145, 175}. Interlayer excitons can be created in electron hole bilayers of TMDs both by electrostatic gating and optical pumping¹⁷⁶⁻¹⁷⁸. Furthermore, in certain cases, one of the electron or hole can be delocalized across the two layers, leading to a hybrid exciton states with characteristics of both interlayer and intralayer excitons^{53, 85, 113, 129, 147, 148}. (b) Energy diagrams of momentum-direct and -indirect excitons.

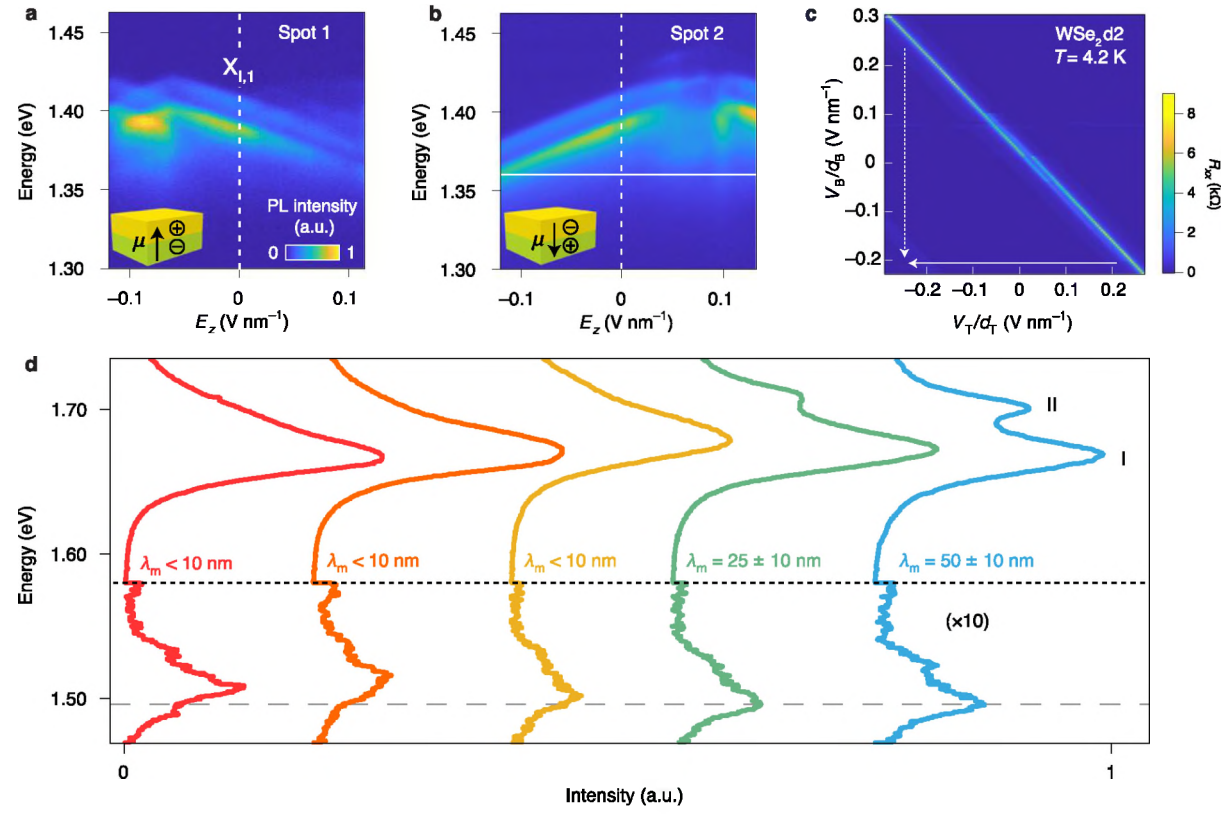


Fig. 8 Experimental observation of excitons in homo-moiré superlattice. a, b, Excitons in the domains of marginally twisted MoSe₂ bilayers exhibit a preferred dipole orientation. Inset: schematic of $X_{I,1}$ with different preferred dipole moment (μ) orientations. All data are collected at 4 K. c, Electric field dependence of the polarization in an R-stacked WSe₂ homobilayer. d, Correlating the optical properties of twisted WSe₂ homobilayer with their moiré lattice constant. λ_m : lattice constant of the moiré superlattice at different positions. The higher-energy K-valley momentum-direct intralayer exciton (type II) emerges as λ_m increases ($\lambda_m > 10$ nm). All data are collected at 4 K. Panels adapted with permission from: a, b, Reproduced with permission from Sung *et al.*, Nat. Nanotechnol. 15, 750-754 (2020). Copyright 2020 Springer Nature Ltd; c, Reproduced with permission from Wang *et al.*, Nat. Nanotechnol. 17, 367-371 (2022). Copyright 2022 Springer Nature Ltd; d, Reproduced with permission from Andersen *et al.*, Nat. Mater. 20, 480-487 (2021). Copyright 2021 Springer Nature Ltd.

This is the author's peer reviewed, accepted manuscript. However, the online version of record will be different from this version once it has been copyedited and typeset PLEASE CITE THIS ARTICLE AS DOI: 10.1063/5.0139179

b 1.0 intensity 2° twist 10 μW PL intensity (a.u.) PL intensity (a.u.) 0 Energy (meV) 20 nW 1,300 1,350 1,400 1.450 1.30 1.32 1.34 1.36 Energy (eV) Emission energy (meV) C d Charge concentration (1012 cm⁻²) 0.16 Reflection contrast (a.u.) 2/3 0.12 1/3 0 n/n 0.08 0 0.5 -1/3 -2/3 0.0 1.65 1.75 -20 0 20 1.70 1.80 -40 Energy (eV) Delay (ns)

Fig. 9 Experimental observation of excitons in hetero-moiré superlattice. a, Evidence of trapped excitons in MoSe₂/WSe₂ heterobilayers with different near-zero twist angles: 1° (bottom) and 2° (top). **b**, Trapped interlayer moiré excitons from a MoSe₂/WSe₂ heterobilayer with a twist angle of 2° at different excitation powers. Inset, a representative PL peak under low excitation power exhibiting narrow linewidth. **c**, Second-order photon correlation statistics show antibunching of interlayer moiré excitons from a MoSe₂/WSe₂ heterobilayer with a twist angle of $\sim 60^\circ$. The $g^{(2)}(0)$ can be revealed by fitting (red solid line). The black dashed line shows the experimental limitation for $g^{(2)}(0)$. **d**, Doping-dependent reflection contrast spectra of a R-stacked WSe₂/WS₂ heterobilayer. Distinct behavior for the intralayer WSe₂ moiré excitons I, II and III can be observed. The shift of peak III under doping is highlighted with white lines for clarity. Panels adapted with permission from: **a**, Reproduced with permission from Tran *et al.*, Nature **567**, 71-75 (2019). Copyright 2019 Springer Nature Ltd; **b**, Reproduced with permission from Seyler *et al.*, Nature **567**, 66-70 (2019). Copyright 2019 Springer Nature Ltd; **c**, Reproduced with permission from Baek *et al.*, Sci. Adv. **6**, eaba8526 (2020). Licensed under a Creative Commons Attribution (CC BY) license; **d**, Reproduced with permission from Naik *et al.*, Nature **609**, 52-57 (2022). Copyright 2022 Springer Nature Ltd.

PLEASE CITE THIS ARTICLE AS DOI: 10.1063/5.0139179

Fig. 10 Advances in controlling twist angles of a moiré system. a-c, AFM-rotatable graphene/hBN heterostructure. Three different orientations of the top BN are displayed (referenced to the AFM coordinate system). d-g, Optical images of a MoS₂ monolayer and twisted MoS₂ bilayers with different twist angles synthesized by CVD method. h, Simulated supertwisted spirals with increasing positive or negative twist angles. i, AFM image of a representative WS₂ supertwisted spiral grown around WO_x particles on a non-Euclidean SiO₂/Si substrate. Panels adapted with permission from: a-c, Reproduced with permission from Ribeiro-Palau *et al.*, Science 361, 690-693 (2018). Licensed under a Creative Commons Attribution (CC BY) license; d-g, Reproduced with permission from Liu *et al.*, Nat. Commun. 5, 4966 (2014). Copyright 2014 Springer Nature Ltd; h, i, Reproduced with permission from Zhao *et al.*, Science 370, 442-445 (2020). Licensed under a Creative Commons Attribution (CC BY) license.

This is the author's peer reviewed, accepted manuscript. However, the online version of record will be different from this version once it has been copyedited and typeset. PLEASE CITE THIS ARTICLE AS DOI: 10.1063/5.0139179

References:

- 1. Mott, N.F. The basis of the electron theory of metals, with special reference to the transition metals. *Proceedings of the Physical Society. Section A* **62**, 416 (1949).
- 2. Imada, M., Fujimori, A. & Tokura, Y. Metal-insulator transitions. *Reviews of modern physics* **70**, 1039 (1998).
- 3. Goodenough, J.B. Metallic oxides. *Prog. Solid State Chem.* **5**, 145-399 (1971).
- 4. Mott, N. Metal-insulator transitions. (CRC Press, 2004).
- 5. Bednorz, J.G. & Müller, K.A. Perovskite-type oxides—the new approach to high-T_c superconductivity. *Reviews of Modern Physics* **60**, 585 (1988).
- 6. Lee, P.A., Nagaosa, N. & Wen, X.-G. Doping a Mott insulator: Physics of high-temperature superconductivity. *Reviews of modern physics* **78**, 17 (2006).
- 7. Rau, J.G. & Gingras, M.J. Frustrated quantum rare-earth pyrochlores. *Annual Review of Condensed Matter Physics* **10**, 357-386 (2019).
- 8. Aetukuri, N.B. *et al.* Control of the metal–insulator transition in vanadium dioxide by modifying orbital occupancy. *Nature Physics* **9**, 661-666 (2013).
- 9. Jaramillo, R., Ha, S.D., Silevitch, D. & Ramanathan, S. Origins of bad-metal conductivity and the insulator-metal transition in the rare-earth nickelates. *Nature Physics* **10**, 304-307 (2014).
- 10. Torrance, J., Lacorre, P., Nazzal, A., Ansaldo, E. & Niedermayer, C. Systematic study of insulator-metal transitions in perovskites RNiO₃ (R= Pr, Nd, Sm, Eu) due to closing of charge-transfer gap. *Physical Review B* **45**, 8209 (1992).
- 11. Middey, S. *et al.* Physics of Ultrathin Films and Heterostructures of Rare-Earth Nickelates. *Annual Review of Materials Research* **46**, 305-334 (2016).
- 12. Yoon, H. *et al.* Reversible phase modulation and hydrogen storage in multivalent VO₂ epitaxial thin films. *Nature materials* **15**, 1113-1119 (2016).
- 13. Cao, J. *et al.* Strain engineering and one-dimensional organization of metal-insulator domains in single-crystal vanadium dioxide beams. *Nature nanotechnology* **4**, 732-737 (2009).
- 14. Shi, J., Zhou, Y. & Ramanathan, S. Colossal resistance switching and band gap modulation in a perovskite nickelate by electron doping. *Nature communications* 5, 1-9 (2014).
- 15. Qin, M., Schäfer, T., Andergassen, S., Corboz, P. & Gull, E. The Hubbard model: A computational perspective. *Annual Review of Condensed Matter Physics* **13**, 275-302 (2022).
- 16. Hubbard, J. Electron correlations in narrow energy bands. *Proceedings of the Royal Society of London. Series A. Mathematical and Physical Sciences* **276**, 238-257 (1963).
- 17. Hubbard, J. Electron correlations in narrow energy bands. II. The degenerate band case. *Proceedings of the Royal Society of London. Series A. Mathematical and Physical Sciences* **277**, 237-259 (1964).
- 18. Hubbard, J. Electron correlations in narrow energy bands III. An improved solution. *Proceedings of the Royal Society of London. Series A. Mathematical and Physical Sciences* **281**, 401-419 (1964).
- 19. Dagotto, E. Complexity in strongly correlated electronic systems. *Science* **309**, 257-262 (2005).

- 20. Zhou, Y. & Ramanathan, S. Mott memory and neuromorphic devices. *Proceedings of the IEEE* **103**, 1289-1310 (2015).
- 21. Tokura, Y., Kawasaki, M. & Nagaosa, N. Emergent functions of quantum materials. *Nature Physics* **13**, 1056-1068 (2017).
- Zaanen, J. & Sawatzky, G. The electronic structure and superexchange interactions in transition-metal compounds. *Can. J. Phys.* **65**, 1262-1271 (1987).
- 23. Kurpas, M., Junior, P.E.F., Gmitra, M. & Fabian, J. Spin-orbit coupling in elemental two-dimensional materials. *Physical Review B* **100**, 125422 (2019).
- 24. Schaibley, J.R. et al. Valleytronics in 2D materials. *Nature Reviews Materials* 1, 1-15 (2016).
- 25. Lee, D. et al. Isostructural metal-insulator transition in VO₂. Science **362**, 1037-1040 (2018).
- 26. Budai, J.D. *et al.* Metallization of vanadium dioxide driven by large phonon entropy. *Nature* **515**, 535-539 (2014).
- 27. Kumar, S., Strachan, J.P. & Williams, R.S. Chaotic dynamics in nanoscale NbO₂ Mott memristors for analogue computing. *Nature* **548**, 318-321 (2017).
- 28. Filinchuk, Y. et al. In situ diffraction study of catalytic hydrogenation of VO₂: Stable phases and origins of metallicity. J. Am. Chem. Soc. **136**, 8100-8109 (2014).
- 29. Chen, J. et al. Revealing the role of lattice distortions in the hydrogen-induced metal-insulator transition of SmNiO₃. Nature communications 10, 1-8 (2019).
- 30. Hofstetter, W. & Qin, T. Quantum simulation of strongly correlated condensed matter systems. *Journal of Physics B: Atomic, Molecular and Optical Physics* **51**, 082001 (2018).
- 31. Imada, M. A quantum simulation study of superconducting correlation in electron systems with strong correlation. *J. Phys. Soc. Jpn.* **57**, 3128-3140 (1988).
- 32. Georgescu, I.M., Ashhab, S. & Nori, F. Quantum simulation. *Reviews of Modern Physics* **86**, 153 (2014).
- 33. Altman, E. *et al.* Quantum simulators: Architectures and opportunities. *PRX Quantum* **2**, 017003 (2021).
- 34. Lloyd, S. Universal quantum simulators. *Science* **273**, 1073-1078 (1996).
- 35. Buluta, I. & Nori, F. Quantum simulators, *Science* **326**, 108-111 (2009).
- 36. Gross, C. & Bloch, I. Quantum simulations with ultracold atoms in optical lattices. *Science* **357**, 995-1001 (2017).
- 37. Zwerger, W. Mott-Hubbard transition of cold atoms in optical lattices. *Journal of Optics B: quantum and semiclassical optics* **5**, S9 (2003).
- 38. Lewenstein, M., Sanpera, A. & Ahufinger, V. *Ultracold Atoms in Optical Lattices: Simulating quantum many-body systems.* (OUP Oxford, 2012).
- 39. Schäfer, F., Fukuhara, T., Sugawa, S., Takasu, Y. & Takahashi, Y. Tools for quantum simulation with ultracold atoms in optical lattices. *Nature Reviews Physics* **2**, 411-425 (2020).
- 40. Wilson, N.P., Yao, W., Shan, J. & Xu, X. Excitons and emergent quantum phenomena in stacked 2D semiconductors. *Nature* **599**, 383-392 (2021).
- 41. Cao, Y. *et al.* Unconventional superconductivity in magic-angle graphene superlattices. *Nature* **556**, 43-50 (2018).
- 42. Park, J.M., Cao, Y., Watanabe, K., Taniguchi, T. & Jarillo-Herrero, P. Flavour Hund's coupling, Chern gaps and charge diffusivity in moiré graphene. *Nature* **592**, 43-48 (2021).

- 43. Morales-Durán, N., Potasz, P. & MacDonald, A.H. Magnetism and Quantum Melting in Moir\'e-Material Wigner Crystals. *arXiv preprint arXiv:2210.15168* (2022).
- 44. Cao, Y. *et al.* Correlated insulator behaviour at half-filling in magic-angle graphene superlattices. *Nature* **556**, 80-84 (2018).
- 45. Xu, Y. *et al.* A tunable bilayer Hubbard model in twisted WSe2. *Nature nanotechnology* **17**, 934-939 (2022).
- 46. McGilly, L.J. *et al.* Visualization of moiré superlattices. *Nature nanotechnology* **15**, 580-584 (2020).
- 47. Bistritzer, R. & MacDonald, A.H. Moiré bands in twisted double-layer graphene. *Proceedings of the National Academy of Sciences* **108**, 12233-12237 (2011).
- 48. Carr, S., Fang, S. & Kaxiras, E. Electronic-structure methods for twisted moiré layers. *Nature Reviews Materials* **5**, 748-763 (2020).
- 49. Chen, G. et al. Evidence of a gate-tunable Mott insulator in a trilayer graphene moiré superlattice. *Nature Physics* **15**, 237-241 (2019).
- 50. Regan, E.C. *et al.* Mott and generalized Wigner crystal states in WSe2/WS2 moiré superlattices. *Nature* **579**, 359-363 (2020).
- 51. Li, T. *et al.* Continuous Mott transition in semiconductor moiré superlattices. *Nature* **597**, 350-354 (2021).
- 52. Tang, Y. et al. Simulation of Hubbard model physics in WSe₂/WS₂ moiré superlattices. *Nature* **579**, 353-358 (2020).
- 53. Wang, L. *et al.* Correlated electronic phases in twisted bilayer transition metal dichalcogenides. *Nature materials* **19**, 861-866 (2020).
- 54. Xu, Y. *et al.* Correlated insulating states at fractional fillings of moiré superlattices. *Nature* **587**, 214-218 (2020).
- 55. Ma, L. *et al.* Strongly correlated excitonic insulator in atomic double layers. *Nature* **598**, 585-589 (2021).
- 56. Chen, D. *et al.* Excitonic insulator in a heterojunction moiré superlattice. *Nature Physics* **18**, 1171-1176 (2022).
- 57. Chhowalla, M. et al. The chemistry of two-dimensional layered transition metal dichalcogenide nanosheets. *Nature chemistry* **5**, 263-275 (2013).
- 58. Geim, A.K. & Grigorieva, I.V. Van der Waals heterostructures. *Nature* **499**, 419-425 (2013).
- 59. Novoselov, K., Mishchenko, o.A., Carvalho, o.A. & Castro Neto, A. 2D materials and van der Waals heterostructures. *Science* **353**, aac9439 (2016).
- 60. Zhou, J. et al. A library of atomically thin metal chalcogenides. *Nature* **556**, 355-359 (2018).
- Zhou, Y. *et al.* Bilayer Wigner crystals in a transition metal dichalcogenide heterostructure. *Nature* **595**, 48-52 (2021).
- 62. Ghiotto, A. *et al.* Quantum criticality in twisted transition metal dichalcogenides. *Nature* **597**, 345-349 (2021).
- 63. Jin, C. *et al.* Observation of moiré excitons in WSe₂/WS₂ heterostructure superlattices. *Nature* **567**, 76-80 (2019).
- 64. Andersen, T.I. *et al.* Excitons in a reconstructed moiré potential in twisted WSe₂/WSe₂ homobilayers. *Nature materials* **20**, 480-487 (2021).
- 65. Liu, Y., Huang, Y. & Duan, X. Van der Waals integration before and beyond two-dimensional materials. *Nature* **567**, 323-333 (2019).

PLEASE CITE THIS ARTICLE AS DOI: 10.1063/5.0139179

- Manzeli, S., Ovchinnikov, D., Pasquier, D., Yazyev, O.V. & Kis, A. 2D transition metal dichalcogenides. *Nature Reviews Materials* 2, 1-15 (2017).
 Liu, G.-B., Xiao, D., Yao, Y., Xu, X. & Yao, W. Electronic structures and theoretical modelling of two-dimensional group-VIB transition metal dichalcogenides. *Chemical*
- Mak, K.F., Lee, C., Hone, J., Shan, J. & Heinz, T.F. Atomically thin MoS 2: a new direct-gap semiconductor. *Physical review letters* **105**, 136805 (2010).

Society Reviews 44, 2643-2663 (2015).

- 69. Splendiani, A. *et al.* Emerging photoluminescence in monolayer MoS₂. *Nano Lett.* **10**, 1271-1275 (2010).
- 70. Xu, S.-Y. *et al.* Electrically switchable Berry curvature dipole in the monolayer topological insulator WTe₂. *Nature Physics* **14**, 900-906 (2018).
- 71. Liu, Y. *et al.* Valleytronics in transition metal dichalcogenides materials. *Nano Research* **12**, 2695-2711 (2019).
- 72. Wilson, N.R. *et al.* Determination of band offsets, hybridization, and exciton binding in 2D semiconductor heterostructures. *Science advances* **3**, e1601832 (2017).
- 73. Wang, G. et al. Colloquium: Excitons in atomically thin transition metal dichalcogenides. *Reviews of Modern Physics* **90**, 021001 (2018).
- 74. Chernikov, A. *et al.* Electrical tuning of exciton binding energies in monolayer WS₂. *Phys. Rev. Lett.* **115**, 126802 (2015).
- 75. Ross, J.S. *et al.* Electrical control of neutral and charged excitons in a monolayer semiconductor. *Nature communications* **4**, 1474 (2013).
- 76. Mak, K.F. *et al.* Tightly bound trions in monolayer MoS₂. *Nature materials* **12**, 207-211 (2013).
- 77. Sidler, M. *et al.* Fermi polaron-polaritons in charge-tunable atomically thin semiconductors. *Nature Physics* **13**, 255-261 (2017).
- 78. Frisenda, R. et al. Recent progress in the assembly of nanodevices and van der Waals heterostructures by deterministic placement of 2D materials. *Chem. Soc. Rev.* 47, 53-68 (2018).
- 79. Castellanos-Gomez, A. *et al.* Deterministic transfer of two-dimensional materials by all-dry viscoelastic stamping. *2D Materials* **1**, 011002 (2014).
- Wang, L. *et al.* One-dimensional electrical contact to a two-dimensional material. *Science* **342**, 614-617 (2013).
- 81. Rhodes, D., Chae, S.H., Ribeiro-Palau, R. & Hone, J. Disorder in van der Waals heterostructures of 2D materials. *Nature materials* **18**, 541-549 (2019).
- 82. Edelberg, D. *et al.* Approaching the intrinsic limit in transition metal diselenides via point defect control. *Nano Lett.* **19**, 4371-4379 (2019).
- 83. Devakul, T., Crépel, V., Zhang, Y. & Fu, L. Magic in twisted transition metal dichalcogenide bilayers. *Nature communications* **12**, 1-9 (2021).
- 84. Li, E. *et al.* Lattice reconstruction induced multiple ultra-flat bands in twisted bilayer WSe₂. *Nature communications* **12**, 1-7 (2021).
- 85. Zhang, L. *et al.* Twist-angle dependence of moiré excitons in WS₂/MoSe₂ heterobilayers. *Nature communications* **11**, 1-8 (2020).
- 86. Nayak, P.K. *et al.* Probing evolution of twist-angle-dependent interlayer excitons in MoSe₂/WSe₂ van der Waals heterostructures. *ACS nano* **11**, 4041-4050 (2017).

- 87. Wilson, J.A. & Yoffe, A. The transition metal dichalcogenides discussion and interpretation of the observed optical, electrical and structural properties. *Advances in Physics* **18**, 193-335 (1969).
- 88. Liu, E. et al. Exciton-polaron Rydberg states in monolayer MoSe₂ and WSe₂. *Nature communications* 12, 1-8 (2021).
- 89. Chernikov, A. et al. Exciton binding energy and nonhydrogenic Rydberg series in monolayer WS₂. Phys. Rev. Lett. 113, 076802 (2014).
- 90. Shimazaki, Y. *et al.* Strongly correlated electrons and hybrid excitons in a moiré heterostructure. *Nature* **580**, 472-477 (2020).
- 91. Smoleński, T. *et al.* Signatures of Wigner crystal of electrons in a monolayer semiconductor. *Nature* **595**, 53-57 (2021).
- 92. Fogler, M., Butov, L. & Novoselov, K. High-temperature superfluidity with indirect excitons in van der Waals heterostructures. *Nature communications* **5**, 1-5 (2014).
- 93. Palacios-Berraquero, C. et al. Large-scale quantum-emitter arrays in atomically thin semiconductors. *Nature communications* **8**, 1-6 (2017).
- 94. Cotrufo, M., Sun, L., Choi, J., Alù, A. & Li, X. Enhancing functionalities of atomically thin semiconductors with plasmonic nanostructures. *Nanophotonics* **8**, 577-598 (2019).
- 95. Liu, X. *et al.* Tuning electron correlation in magic-angle twisted bilayer graphene using Coulomb screening. *Science* **371**, 1261-1265 (2021).
- 96. Forsythe, C. *et al.* Band structure engineering of 2D materials using patterned dielectric superlattices. *Nature nanotechnology* **13**, 566-571 (2018).
- 97. Yoo, H. *et al.* Atomic and electronic reconstruction at the van der Waals interface in twisted bilayer graphene. *Nature materials* **18**, 448-453 (2019).
- 98. Alden, J.S. *et al.* Strain solitons and topological defects in bilayer graphene. *Proceedings of the National Academy of Sciences* **110**, 11256-11260 (2013).
- 299. Zhang, C. *et al.* Interlayer couplings, Moiré patterns, and 2D electronic superlattices in MoS₂/WSe₂ hetero-bilayers. *Science advances* **3**, e1601459 (2017).
- 100. Kerelsky, A. *et al.* Maximized electron interactions at the magic angle in twisted bilayer graphene. *Nature* **572**, 95-100 (2019).
- 101. Kang, K. *et al.* Layer-by-layer assembly of two-dimensional materials into wafer-scale heterostructures. *Nature* **550**, 229-233 (2017).
- 102. Weston, A. *et al.* Atomic reconstruction in twisted bilayers of transition metal dichalcogenides. *Nature nanotechnology* **15**, 592-597 (2020).
- 103. Yu, H., Liu, G.-B., Tang, J., Xu, X. & Yao, W. Moiré excitons: From programmable quantum emitter arrays to spin-orbit-coupled artificial lattices. *Science advances* 3, e1701696 (2017).
- Wu, F., Lovorn, T. & MacDonald, A. Theory of optical absorption by interlayer excitons in transition metal dichalcogenide heterobilayers. *Physical Review B* **97**, 035306 (2018).
- 105. Wu, F., Lovorn, T. & MacDonald, A.H. Topological exciton bands in moiré heterojunctions. *Phys. Rev. Lett.* **118**, 147401 (2017).
- 106. Angeli, M. & MacDonald, A.H. Γ valley transition metal dichalcogenide moiré bands. *Proceedings of the National Academy of Sciences* **118**, e2021826118 (2021).
- 107. Wu, F., Lovorn, T., Tutuc, E. & MacDonald, A.H. Hubbard model physics in transition metal dichalcogenide moiré bands. *Phys. Rev. Lett.* **121**, 026402 (2018).
- 108. Yankowitz, M. *et al.* Dynamic band-structure tuning of graphene moiré superlattices with pressure. *Nature* **557**, 404-408 (2018).

- 109. Trolle, M.L., Pedersen, T.G. & Véniard, V. Model dielectric function for 2D semiconductors including substrate screening. *Sci. Rep.* 7, 1-9 (2017).
- 110. Raja, A. *et al.* Coulomb engineering of the bandgap and excitons in two-dimensional materials. *Nature communications* **8**, 1-7 (2017).
- 111. Serlin, M. *et al.* Intrinsic quantized anomalous Hall effect in a moiré heterostructure. *Science* **367**, 900-903 (2020).
- 112. Spanton, E.M. *et al.* Observation of fractional Chern insulators in a van der Waals heterostructure. *Science* **360**, 62-66 (2018).
- 113. Scuri, G. et al. Electrically tunable valley dynamics in twisted WSe₂/WSe₂ bilayers. *Phys. Rev. Lett.* **124**, 217403 (2020).
- 114. Cao, Y. *et al.* Tunable correlated states and spin-polarized phases in twisted bilayer–bilayer graphene. *Nature* **583**, 215-220 (2020).
- 115. Li, T. *et al.* Quantum anomalous Hall effect from intertwined moiré bands. *Nature* **600**, 641-646 (2021).
- 116. Tang, Y. *et al.* Dielectric catastrophe at the Wigner-Mott transition in a moiré superlattice. *Nature communications* **13**, 1-7 (2022).
- 117. Allain, A., Kang, J., Banerjee, K. & Kis, A. Electrical contacts to two-dimensional semiconductors. *Nature materials* **14**, 1195-1205 (2015).
- 118. Miao, S. *et al.* Strong interaction between interlayer excitons and correlated electrons in WSe₂/WS₂ moiré superlattice. *Nature communications* **12**, 1-6 (2021).
- 119. Shimazaki, Y. et al. Optical signatures of periodic charge distribution in a Mott-like correlated insulator state. *Physical Review X* 11, 021027 (2021).
- 120. Gao, S., Liang, Y., Spataru, C.D. & Yang, L. Dynamical excitonic effects in doped two-dimensional semiconductors. *Nano Lett.* **16**, 5568-5573 (2016).
- 121. Joglekar, Y.N., Balatsky, A.V. & Sarma, S.D. Wigner supersolid of excitons in electron-hole bilayers. *Physical Review B* **74**, 233302 (2006).
- Huang, D., Choi, J., Shih, C.-K. & Li, X. Excitons in semiconductor moiré superlattices. *Nature nanotechnology* **17**, 227-238 (2022).
- Naik, M.H. *et al.* Intralayer charge-transfer moiré excitons in van der Waals superlattices. *Nature* **609**, 52-57 (2022).
- Yu, H., Liu, G.-B. & Yao, W. Brightened spin-triplet interlayer excitons and optical selection rules in van der Waals heterobilayers. 2D Materials 5, 035021 (2018).
- 125. Perczel, J. *et al.* Topological quantum optics in two-dimensional atomic arrays. *Phys. Rev. Lett.* **119**, 023603 (2017).
- 126. Liu, K. *et al.* Evolution of interlayer coupling in twisted molybdenum disulfide bilayers. *Nature communications* **5**, 1-6 (2014).
- Wu, B. *et al.* Evidence for moiré intralayer excitons in twisted WSe₂/WSe₂ homobilayer superlattices. *Light: Science & Applications* 11, 1-8 (2022).
- 128. Zhao, X. et al. Strong Moiré Excitons in High-Angle Twisted Transition Metal Dichalcogenide Homobilayers with Robust Commensuration. Nano Lett. 22, 203-210 (2021).
- 129. Brem, S. *et al.* Hybridized intervalley moiré excitons and flat bands in twisted WSe₂ bilayers. *Nanoscale* **12**, 11088-11094 (2020).
- 130. Leisgang, N. et al. Giant Stark splitting of an exciton in bilayer MoS₂. Nature nanotechnology **15**, 901-907 (2020).

- Paradisanos, I. *et al.* Controlling interlayer excitons in MoS₂ layers grown by chemical vapor deposition. *Nature communications* **11**, 2391 (2020).
- 132. Van Der Zande, A.M. *et al.* Tailoring the electronic structure in bilayer molybdenum disulfide via interlayer twist. *Nano Lett.* **14**, 3869-3875 (2014).
- 133. Sung, J. *et al.* Broken mirror symmetry in excitonic response of reconstructed domains in twisted MoSe₂/MoSe₂ bilayers. *Nature nanotechnology* **15**, 750-754 (2020).
- Wang, X. *et al.* Interfacial ferroelectricity in rhombohedral-stacked bilayer transition metal dichalcogenides. *Nature nanotechnology* **17**, 367-371 (2022).
- 135. Weston, A. *et al.* Interfacial ferroelectricity in marginally twisted 2D semiconductors. *Nature nanotechnology* **17**, 390-395 (2022).
- 136. Debbichi, L., Eriksson, O. & Lebègue, S. Electronic structure of two-dimensional transition metal dichalcogenide bilayers from ab initio theory. *Physical Review B* **89**, 205311 (2014).
- 137. Komsa, H.-P. & Krasheninnikov, A.V. Electronic structures and optical properties of realistic transition metal dichalcogenide heterostructures from first principles. *Physical Review B* **88**, 085318 (2013).
- 138. Kang, J., Li, J., Li, S.-S., Xia, J.-B. & Wang, L.-W. Electronic structural Moiré pattern effects on MoS₂/MoSe₂ 2D heterostructures. *Nano Lett.* **13**, 5485-5490 (2013).
- 139. Rivera, P. et al. Observation of long-lived interlayer excitons in monolayer MoSe₂–WSe₂ heterostructures. *Nature communications* **6**, 1-6 (2015).
- Lee, C.-H. *et al.* Atomically thin p–n junctions with van der Waals heterointerfaces. *Nature nanotechnology* **9**, 676-681 (2014).
- 141. Furchi, M.M., Pospischil, A., Libisch, F., Burgdörfer, J. & Mueller, T. Photovoltaic effect in an electrically tunable van der Waals heterojunction. *Nano Lett.* **14**, 4785-4791 (2014).
- 142. Cheng, R. et al. Electroluminescence and photocurrent generation from atomically sharp WSe₂/MoS₂ heterojunction p–n diodes. *Nano Lett.* **14**, 5590-5597 (2014).
- 143. Fang, H. *et al.* Strong interlayer coupling in van der Waals heterostructures built from single-layer chalcogenides. *Proceedings of the National Academy of Sciences* **111**, 6198-6202 (2014).
- 144. Tran, K. *et al.* Evidence for moiré excitons in van der Waals heterostructures. *Nature* **567**, 71-75 (2019).
- 145. Seyler, K.L. *et al.* Signatures of moiré-trapped valley excitons in MoSe₂/WSe₂ heterobilayers. *Nature* **567**, 66-70 (2019).
- Baek, H. *et al.* Highly energy-tunable quantum light from moiré-trapped excitons. *Science advances* **6**, eaba8526 (2020).
- 147. Alexeev, E.M. *et al.* Resonantly hybridized excitons in moiré superlattices in van der Waals heterostructures. *Nature* **567**, 81-86 (2019).
- 148. Tang, Y. et al. Tuning layer-hybridized moiré excitons by the quantum-confined Stark effect. *Nature nanotechnology* **16**, 52-57 (2021).
- Ribeiro-Palau, R. *et al.* Twistable electronics with dynamically rotatable heterostructures. *Science* **361**, 690-693 (2018).
- 150. Yao, K. *et al.* Enhanced tunable second harmonic generation from twistable interfaces and vertical superlattices in boron nitride homostructures. *Science Advances* 7, eabe8691 (2021).
- 151. Kapfer, M. et al. Programming moiré patterns in 2D materials by bending. arXiv preprint arXiv:2209.10696 (2022).

- 152. Purdie, D. et al. Cleaning interfaces in layered materials heterostructures. *Nature communications* **9**, 1-12 (2018).
- 153. Lu, X. *et al.* Superconductors, orbital magnets and correlated states in magic-angle bilayer graphene. *Nature* **574**, 653-657 (2019).
- 154. Argentero, G. *et al.* Unraveling the 3D atomic structure of a suspended graphene/hBN van der Waals heterostructure. *Nano Lett.* **17**, 1409-1416 (2017).
- 155. Aslan, B. *et al.* Excitons in strained and suspended monolayer WSe₂. *2D Materials* **9**, 015002 (2021).
- Bunch, J.S. *et al.* Electromechanical resonators from graphene sheets. *Science* **315**, 490-493 (2007).
- 157. Bolotin, K.I. *et al.* Ultrahigh electron mobility in suspended graphene. *Solid State Commun.* **146**, 351-355 (2008).
- 258. Zhou, Y. *et al.* Controlling excitons in an atomically thin membrane with a mirror. *Phys. Rev. Lett.* **124**, 027401 (2020).
- 159. Lemme, M.C. *et al.* Nanoelectromechanical sensors based on suspended 2D materials. *Research* **2020** (2020).
- Song, T. *et al.* Direct visualization of magnetic domains and moiré magnetism in twisted 2D magnets. *Science* **374**, 1140-1144 (2021).
- 161. Chen, D. *et al.* Tuning moiré excitons and correlated electronic states through layer degree of freedom. *Nature communications* **13**, 1-8 (2022).
- Brown, L. *et al.* Twinning and twisting of tri-and bilayer graphene. *Nano Lett.* **12**, 1609-1615 (2012).
- 163. Havener, R.W., Zhuang, H., Brown, L., Hennig, R.G. & Park, J. Angle-resolved Raman imaging of interlayer rotations and interactions in twisted bilayer graphene. *Nano Lett.* **12**, 3162-3167 (2012).
- 2hao, Y. *et al.* Supertwisted spirals of layered materials enabled by growth on non-Euclidean surfaces. *Science* **370**, 442-445 (2020).
- 165. Zhu, S., Pochet, P. & Johnson, H.T. Controlling rotation of two-dimensional material flakes. *ACS nano* **13**, 6925-6931 (2019).
- Bording, J., Li, B., Shi, Y. & Zuo, J. Size-and shape-dependent energetics of nanocrystal interfaces: Experiment and simulation. *Phys. Rev. Lett.* **90**, 226104 (2003).
- 167. Savary, L. & Balents, L. Quantum spin liquids: a review. Rep. Prog. Phys. 80, 016502 (2016).
- Platzman, P. & Dykman, M. Quantum computing with electrons floating on liquid helium. *Science* **284**, 1967-1969 (1999).
- 169. Ciarrocchi, A., Tagarelli, F., Avsar, A. & Kis, A. Excitonic devices with van der Waals heterostructures: valleytronics meets twistronics. *Nature Reviews Materials* 7, 449-464 (2022).
- 170. Choi, J. et al. Moiré potential impedes interlayer exciton diffusion in van der Waals heterostructures. Science advances 6, eaba8866 (2020).
- 171. Zhang, L. *et al.* Van der Waals heterostructure polaritons with moiré-induced nonlinearity. *Nature* **591**, 61-65 (2021).
- 172. Datta, B. et al. Highly nonlinear dipolar exciton-polaritons in bilayer MoS₂. Nature communications 13, 1-7 (2022).

- 173. Li, W., Lu, X., Dubey, S., Devenica, L. & Srivastava, A. Dipolar interactions between localized interlayer excitons in van der Waals heterostructures. *Nature materials* **19**, 624-629 (2020).
- 174. Förg, M. *et al.* Cavity-control of interlayer excitons in van der Waals heterostructures. *Nature communications* **10**, 1-6 (2019).
- 175. Miller, B. *et al.* Long-lived direct and indirect interlayer excitons in van der Waals heterostructures. *Nano Lett.* **17**, 5229-5237 (2017).
- 176. Jauregui, L.A. *et al.* Electrical control of interlayer exciton dynamics in atomically thin heterostructures. *Science* **366**, 870-875 (2019).
- 177. Mahdikhanysarvejahany, F. *et al.* Localized Interlayer Excitons in MoSe₂-WSe₂ Heterostructures without a Moiré Potential. *arXiv preprint arXiv:2203.08052* (2022).
- 178. Förg, M. *et al.* Moiré excitons in MoSe₂-WSe₂ heterobilayers and heterotrilayers. *Nature communications* **12**, 1-7 (2021).



ACCEPTED MANUSCRIPT

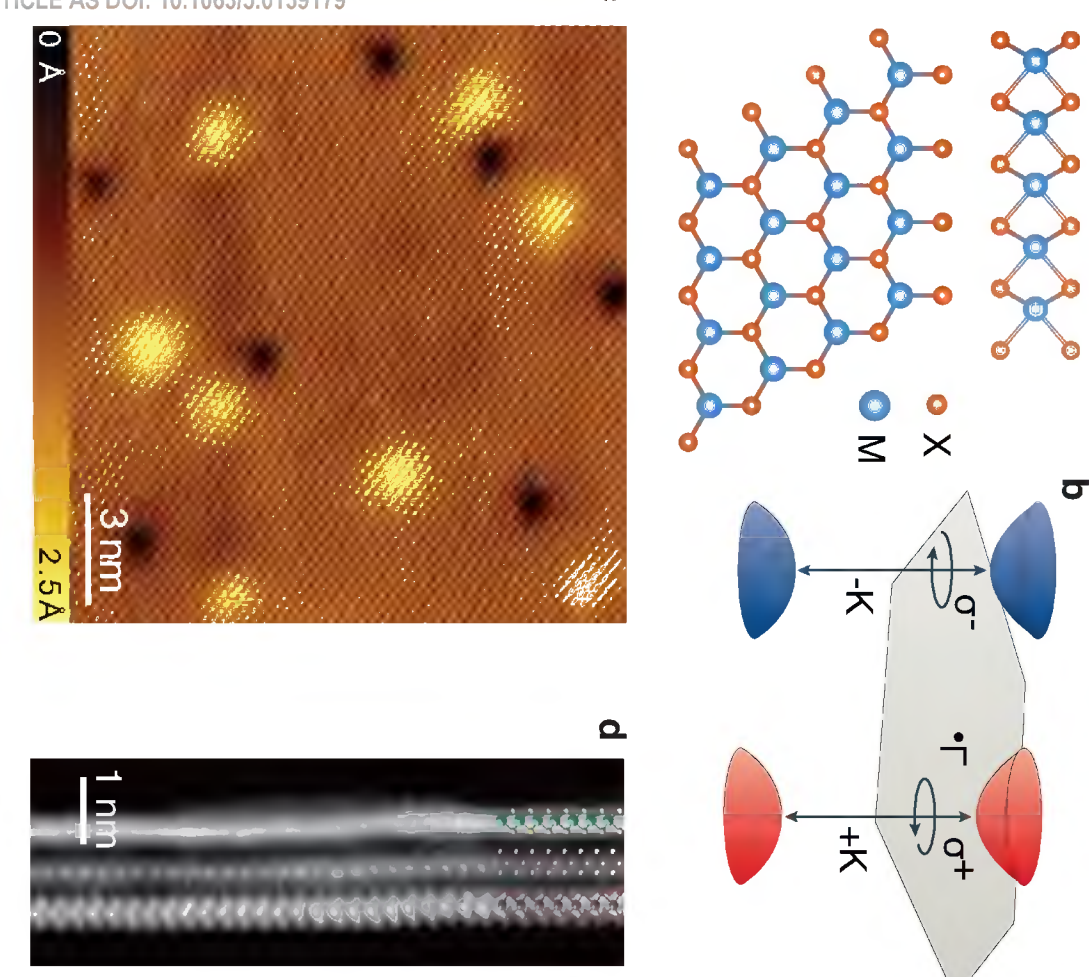
This is the author's peer reviewed, accepted manuscript. However, the online version of record will be viffed extremed this version once it has been copyedited and typeset. moiré exciton superconductivity excitonic insulator correlation moiré $-\mu < 0$ generalized Wigner crystal frustrated magnetism 0 0 Mott insulator

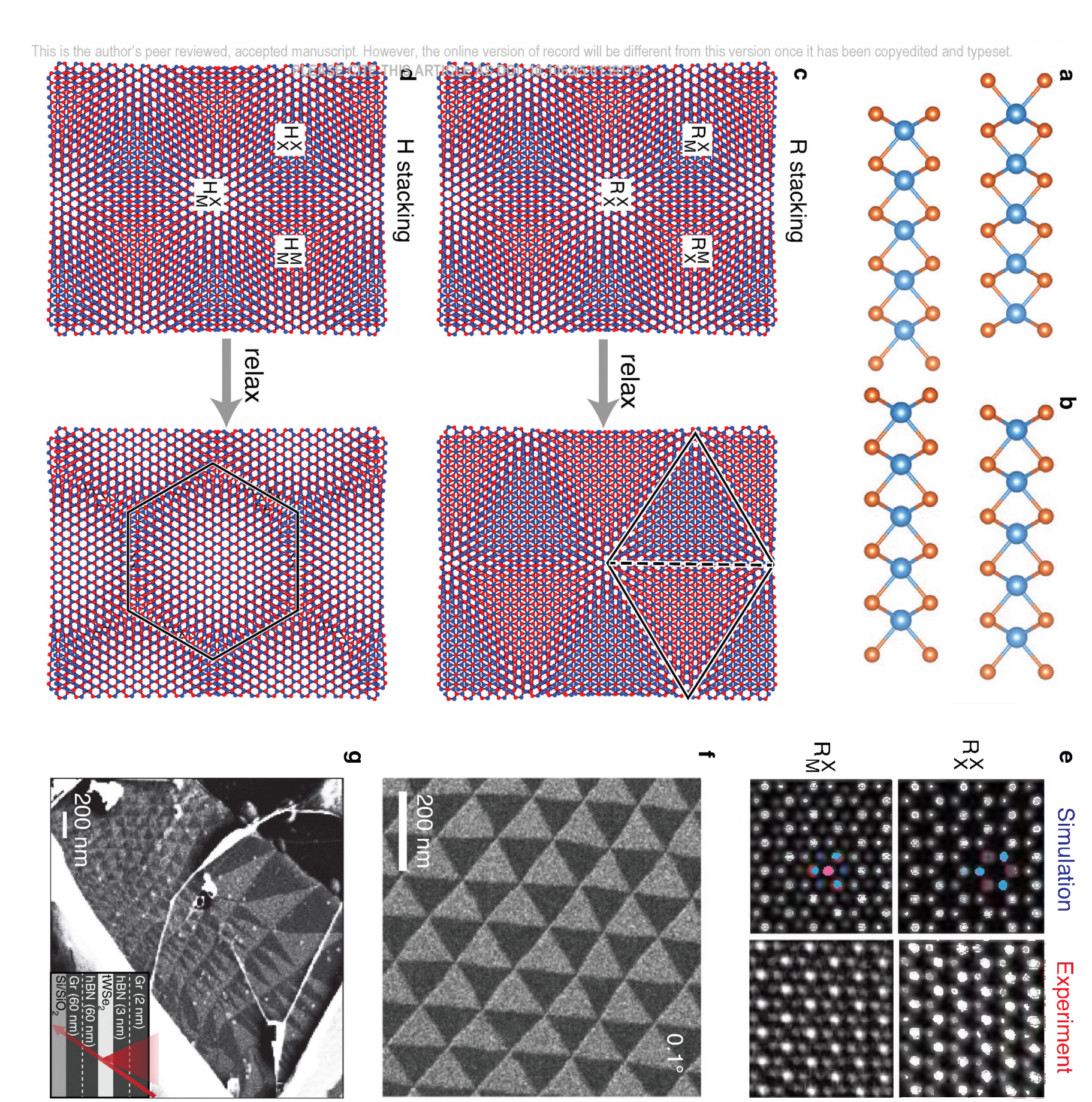


ACCEPTED MANUSCRIPT

This is the author's peer reviewed, accepted manuscript. However, the online version of record will be different from this version once it has been copyedited and typeset.

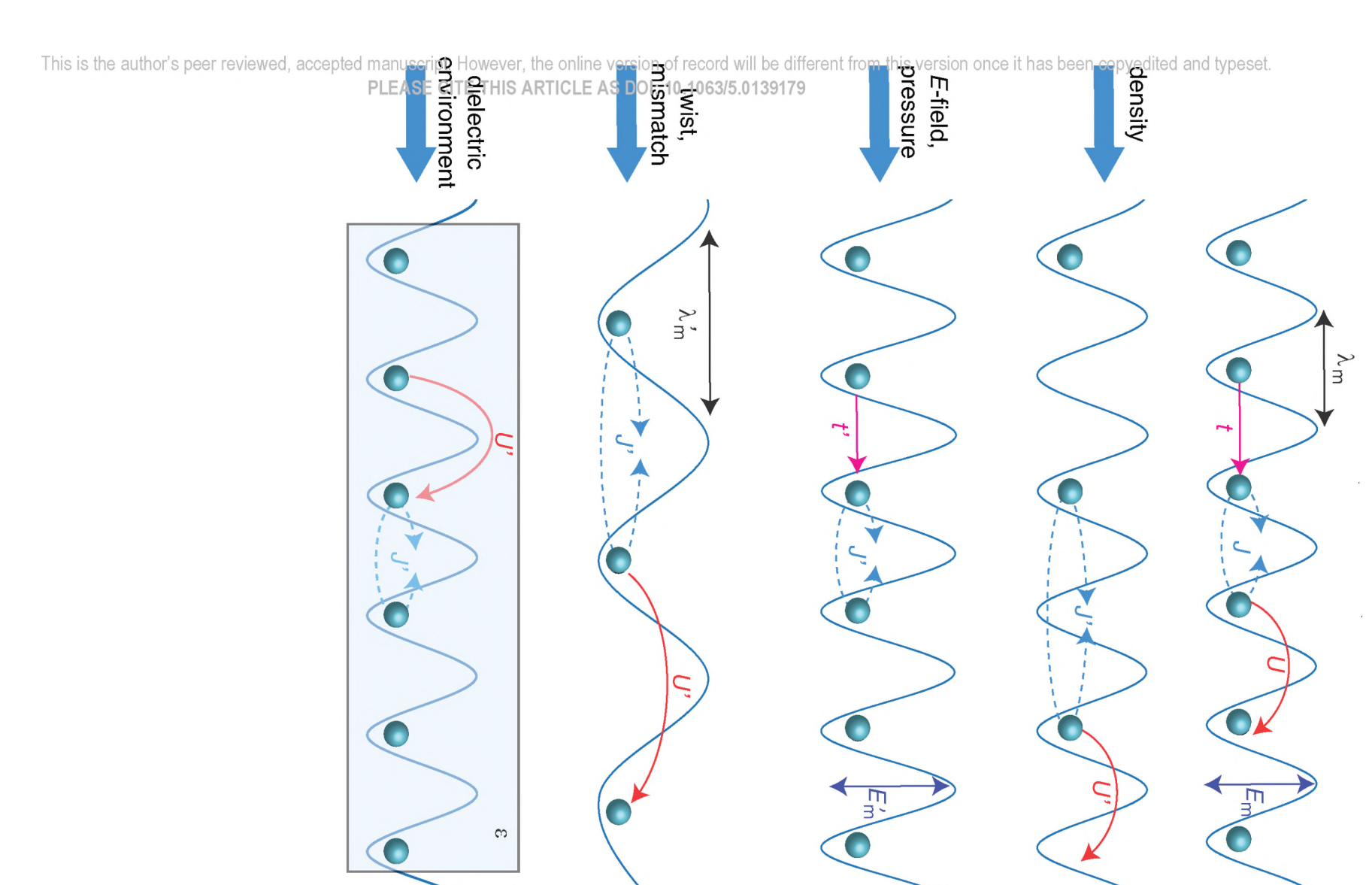
PLEASE CITE THIS ARTICLE AS DOI: 10.1063/5.0139179



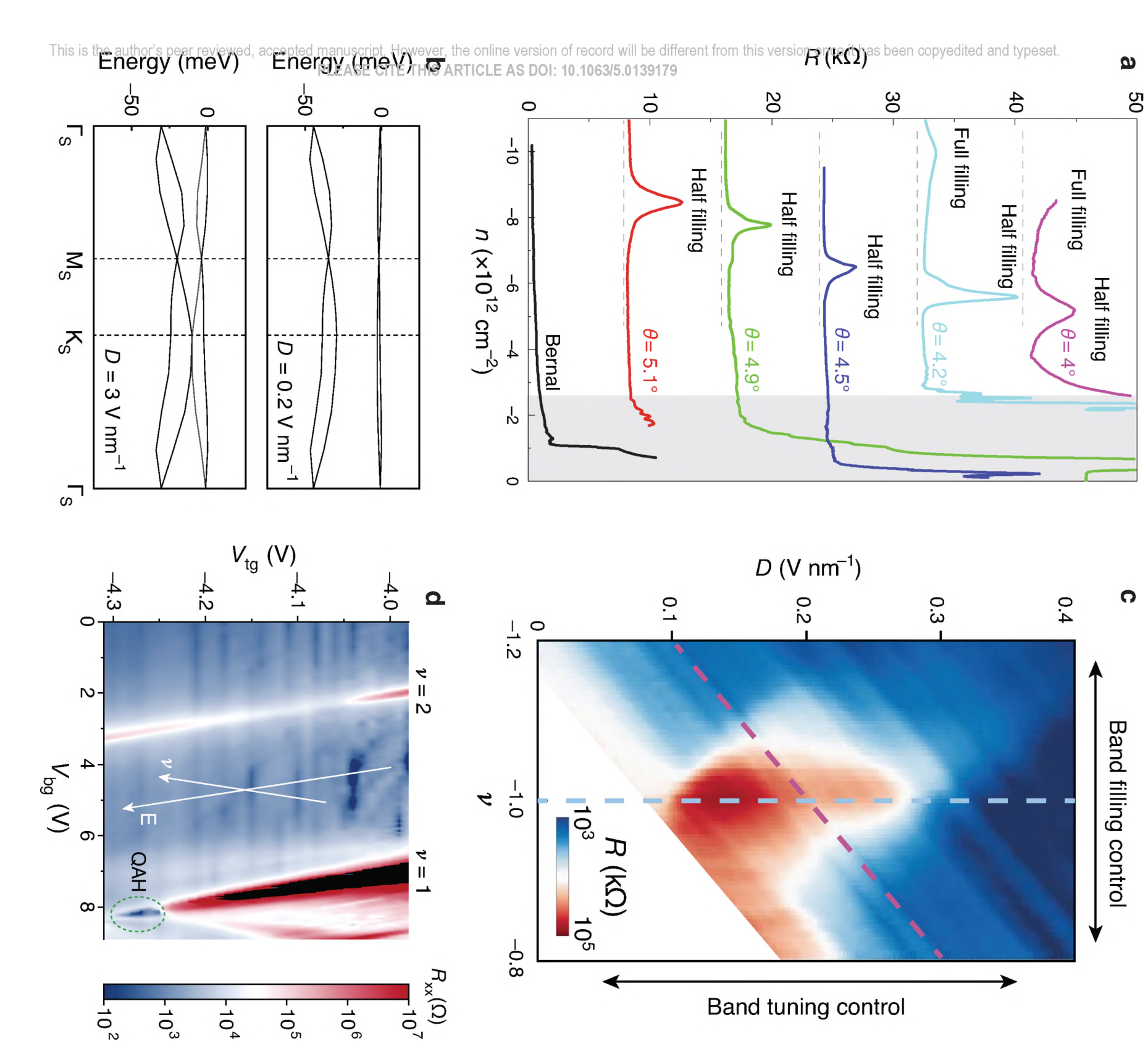


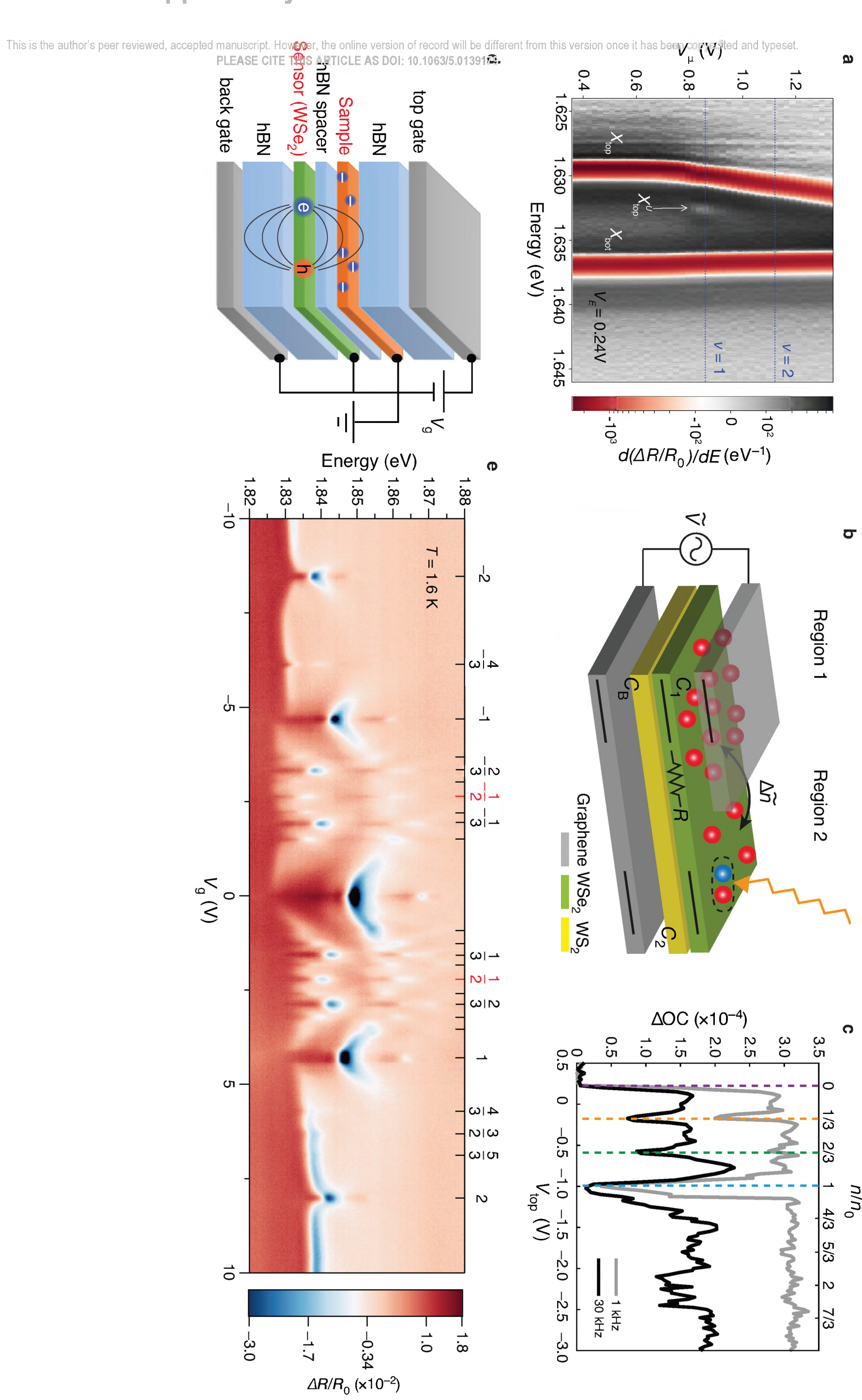


ACCEPTED MANUSCRIPT



ACCEPTED MANUSCRIPT



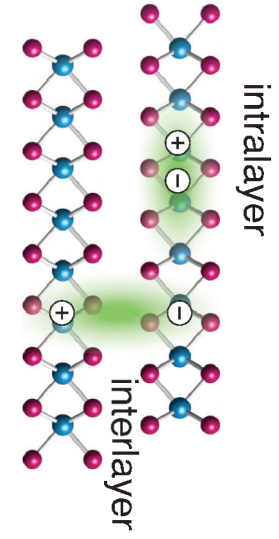


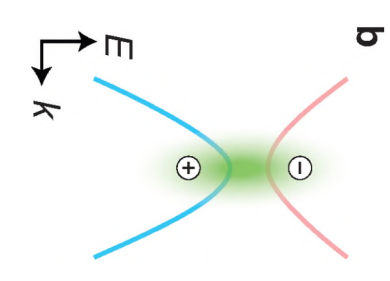


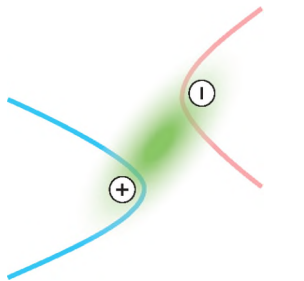
ACCEPTED MANUSCRIPT

This is the author's peer reviewed, accepted manuscript. However, the online version of record will be different from this version once it has been copyedited and typeset.

PLEASE CITE THIS ARTICLE AS DOI: 10.1063/5.0139179

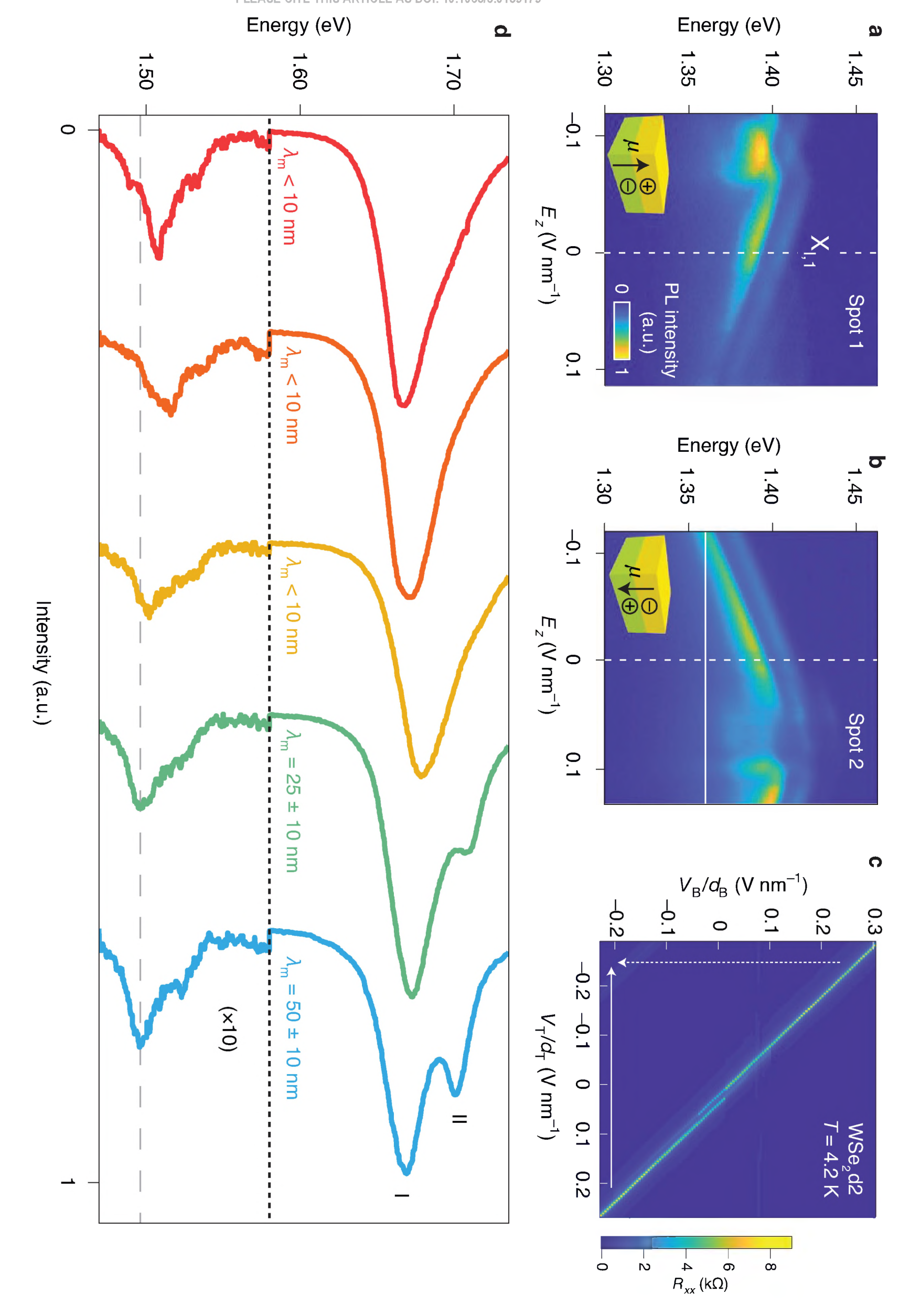




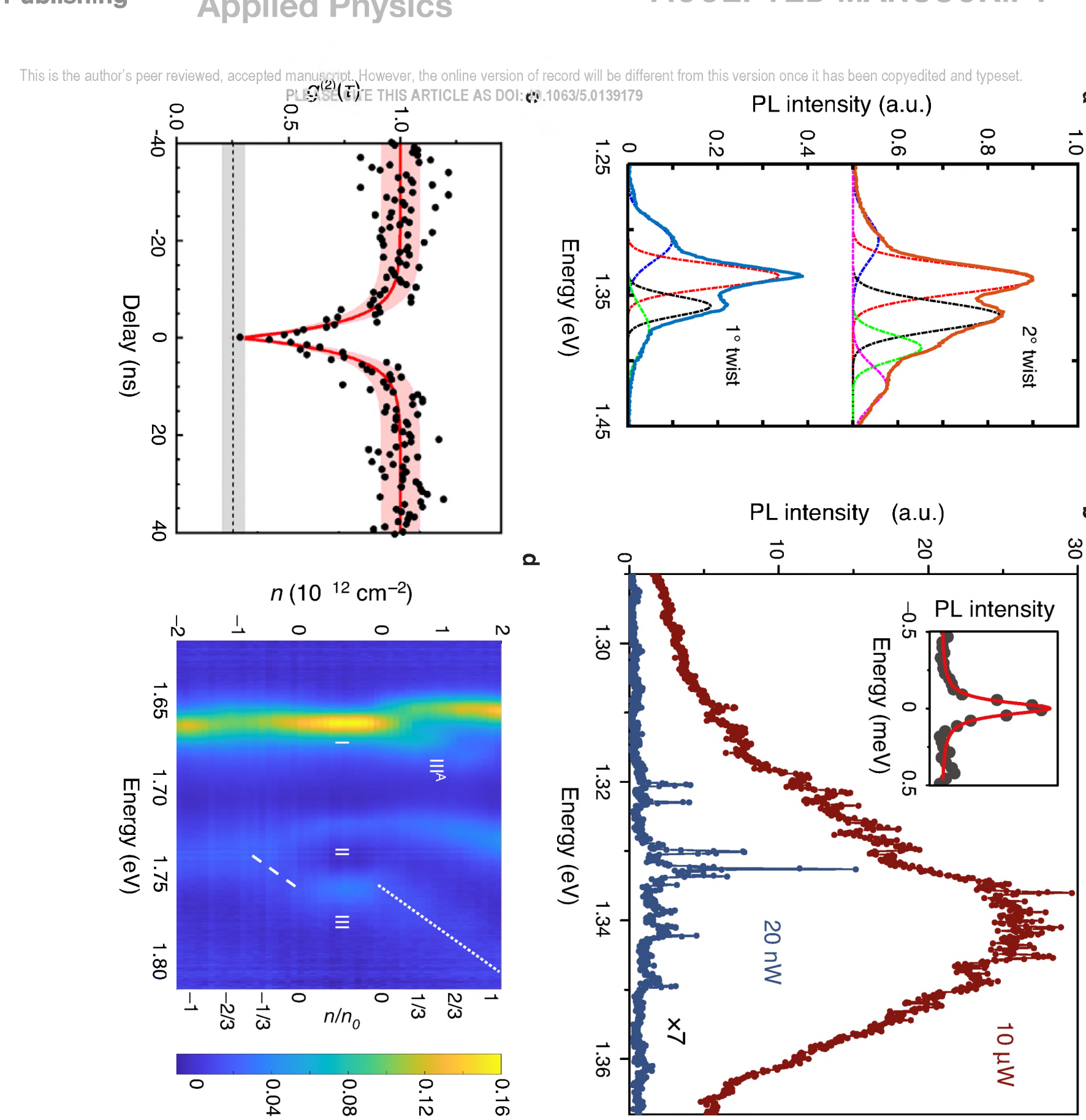


This is the author's peer reviewed, accepted manuscript. However, the online version of record will be different from this version once it has been copyedited and typeset.

PLEASE CITE THIS ARTICLE AS DOI: 10.1063/5.0139179



Reflection contrast (a.u.)





ACCEPTED MANUSCRIPT

This is the author's peer reviewed, accepted manuscript. However, the online version of record will be different from this version once it has been copyedited and typeset.

PLEASE DESCRIPTION OF THE OFFICE AS DESCRIPTIO Ø 10 µm ယွ Φ -5° 5 -15° 15° 9